INFORMATION TO USERS

This material was produced from a microfilm copy of the original document. While the most advanced technological means to photograph and reproduce this document have been used, the quality is heavily dependent upon the quality of the original submitted.

The following explanation of techniques is provided to help you understand markings or patterns which may appear on this reproduction.

1. The sign or "target" for pages apparently lacking from the document photographed is "Missing Page(s)". If it was possible to obtain the missing page(s) or section, they are spliced into the film along with adjacent pages. This may have necessitated cutting thru an image and duplicating adjacent pages to insure you complete continuity.

2. When an image on the film is obliterated with a large round black mark, it is an indication that the photographer suspected that the copy may have moved during exposure and thus cause a blurred image. You will find a good image of the page in the adjacent frame.

3. When a map, drawing or chart, etc., was part of the material being photographed the photographer followed a definite method in "sectioning" the material. It is customary to begin photoing at the upper left hand corner of a large sheet and to continue photoing from left to right in equal sections with a small overlap. If necessary, sectioning is continued again – beginning below the first row and continuing on until complete.

4. The majority of users indicate that the textual content is of greatest value, however, a somewhat higher quality reproduction could be made from "photographs" if essential to the understanding of the dissertation. Silver prints of "photographs" may be ordered at additional charge by writing the Order Department, giving the catalog number, title, author and specific pages you wish reproduced.

5. PLEASE NOTE: Some pages may have indistinct print. Filmed as received.

**Xerox University Microfilms**
300 North Zeeb Road
Ann Arbor, Michigan 48106

76-19,106

CHAPMAN, David Spencer, 1942-
HEAT FLOW AND HEAT PRODUCTION IN ZAMBIA.

The University of Michigan, Ph.D., 1976
Geophysics

**Xerox University Microfilms,** Ann Arbor, Michigan 48106

# HEAT FLOW AND HEAT PRODUCTION IN ZAMBIA

by

David Spencer Chapman

A dissertation submitted in partial fulfillment
of the requirements for the degree of
Doctor of Philosophy
(Geology)
in The University of Michigan
1976

Doctoral Committee:

Professor Henry N. Pollack, Chairman
Associate Professor Bruce R. Clark
Professor George W. Ford
Professor E. William Heinrich
Associate Professor Rob Van der Voo
Professor James T. Wilson

## ACKNOWLEDGMENTS

I wish to thank Professor Henry N. Pollack for introducing me to the discipline of geophysics and for his close guidance throughout this study. I also appreciate the assistance given me by other members of my doctoral committee.

This project was initiated while I was at the University of Zambia. The fieldwork could not have been completed without the cooperation of my colleagues there, and of geologists too numerous to mention from the Geological Survey of Zambia, Nchanga Consolidated Copper Mines, Roan Consolidated Mines, Mkushi Copper Mines, AGIP (Zambia), and MINDECO. In particular, I thank Professors A. H. Ward and C. J. Ball of the University of Zambia for their support and encouragement in the initial stages of this project.

Professor R. F. Roy made the radiogenic heat production measurements. Derwin Bell is responsible for those figures with a professional appearance. Financial support was provided by the University of Zambia, The University of Michigan through a Horace H. Rackham Predoctoral Fellowship, and the US National Science Foundation, Earth Science Section, under Grant GA-36360.

TABLE OF CONTENTS

ACKNOWLEDGMENTS . . . . . ii

LIST OF TABLES . . . . . iv

LIST OF ILLUSTRATIONS . . . . . v

LIST OF APPENDICES . . . . . vi

Chapter

I. INTRODUCTION . . . . . 1

II. GEOTHERMAL MEASUREMENTS AND DATA REDUCTION . . . . . 5

Temperature
Thermal Conductivity
Heat Flow
Heat Production

III. INTERPRETATION OF HEAT-FLOW AND HEAT-PRODUCTION RESULTS . . 30

Tectonic Setting and the Heat-Flow Anomaly
Effect of a Radioactive Surface Layer
Thermal Models and their Geodynamic Implications
Contemporary Tectonics of the African Rift System
Comparison of Rift Tectonics

IV. CONCLUSIONS . . . . . 52

APPENDIX . . . . . 54

REFERENCES . . . . . 89

LIST OF TABLES


| Table | | Page |
|---|---|---|
| 1. | Zambia Heat-Flow Data | 13 |
| 2. | Geochronology and Lithostratigraphic Classification for Central Africa | 18 |
| 3. | Heat-Production Results from Heat-Flow Sites | 27 |
| 4. | Heat-Production Results from Granitic Bodies | 29 |
| 5. | Values of the Dimensionless Parameter K$\ell$ | 42 |
| 6. | Geological and Geophysical Comparison of Modern Rifts | 48 |
| 7. | Thermistor Calibration Constants and Drift Characteristics | 57 |
| 8. | Divided Bar Calibration Constants | 66 |
| 9. | Comparison of Disc Thermal Conductivity Values Corrected for Diameter Mismatch | 67 |

## LIST OF ILLUSTRATIONS


| Figure | | Page |
|---|---|---|
| 1. | Tectonics of East and Central Africa . . . . . | 3 |
| 2. | Temperature-Depth Curves at Selected Heat-Flow Sites . . | 8 |
| 3. | A Comparison of Thermal Conductivity Values Measured at Four Geothermal Laboratories . . . . . | 11 |
| 4. | Bullard Plot of Temperature versus Thermal Resistance. . | 16 |
| 5. | Thermal Regime of Luanshya Mine . . . . . | 23 |
| 6. | Distribution of Zambia Heat-Flow Sites . . . . . | 32 |
| 7. | Continental Heat Flow Variation with Age of Last Tectono-Thermal Event . . . . . | 33 |
| 8. | Heat Flow and Heat Production in Zambia | 36 |
| 9. | Thermal Models for a Temperature Perturbation at the Base of the Lithosphere . . . . . | 40 |
| 10. | Rift Valley Heat Flow . . . . . | 49 |
| 11. | Thermistor Probe Assembly . . . . . | 55 |
| 12. | Circuit Diagram for Resistance Bridge . . . . . | 60 |
| 13. | Divided Bar Thermal Conductivity Apparatus . . . . . | 61 |

LIST OF APPENDICES


| Appendix | | Page |
|---|---|---|
| I. | Construction and Calibration of Heat-Flow Equipment . . . . . | 54 |
| | Temperature Probes<br>Thermistor Calibration and Stability<br>Cables and Reel<br>Resistance Bridge<br>Divided Bar Construction<br>Calibration of the Divided Bar<br>Corrections for Undersized and Oversized Disks | |
| II. | Heat Flow Data from Zambia . . . . . | 69 |

# CHAPTER I

## INTRODUCTION

Knowledge of the thermal state of the lithosphere plays an important, if not fundamental, role in modern theories of geodynamic processes, and surface heat-flow measurements provide the most direct indications of the regional variation of thermal conditions at shallow depths within the earth. In this paper I describe the results of a program of heat-flow measurements on the Central African plateau, undertaken with the dual purpose of extending the heat-flow coverage on the African continent and providing some constraints on geodynamic models of continental rifting.

Notwithstanding Bullard's pioneering heat-flow work in South Africa (Bullard, 1939), and subsequent work there and in South West Africa by Carte (1954), Gough (1963), and Carte and van Rooyen (1971), until 1967 not a single continental heat-flow result had been published for Africa north of the Limpopo river. Since that time, Beck and Mustonen (1972), Chapman and Pollack (1974), and Sass and Behrendt (1975) have conducted measurements in parts of West Africa. In East Africa, Girdler (1969) and Evans and Tammemagi (1974) have reported heat-flow values from the coastal plains of Sudan and Somalia, and Morgan et al. (1973) have conducted heat-flow surveys in and near the Gregory rift in Kenya. Oceanographic techniques have been utilized to make heat-flow measurements in the rift Lakes Malawi, Tanganyika, and Kivu (Von Herzen and

Vacquier, 1967; Degens et al., 1971; Degens, et al., 1973), but unfortunately the large scatter in these lake data makes interpretation of the results difficult. The existing set of African measurements can be characterized as follows: the lowest African heat-flow values lie within the older shields of West and South Africa, whereas higher values occur in the younger regions of the southern Karroo Basin, the Somalia Horm and northeast Sudan; normal to high heat flow is observed within the eastern rift valley of Kenya and normal heat flow on the rift flanks.

Prior to the results reported herein, there were no continental heat-flow measurements between the Gregory rift in Kenya and the Republic of South Africa. This region, from $5^{\circ}$ to $25^{\circ}$S and $20^{\circ}$ to $35^{\circ}$E, is one of considerable tectonic interest, largely because of the presence of the East African rift system in the eastern part of the region, and because of speculations of a possible southwestward continuation of the rift (Fairhead and Girdler, 1969; Scholz, 1975). The general location of the region together with some geologic and geophysical indicators of contemporary tectonism is shown in Figure 1. Although the western rift system finds topographic expression in a roughly south-by-southeast line through Lakes Tanganyika, Rukwa, and Malawi, there is a growing body of geophysical evidence that suggests the presence of one or several arms of the rift system extending along southwest trends across the Central African plateau, through the Republic of Zambia and northern Botswana. A recently discovered electrical conductivity anomaly (de Beer, et al., 1975), and preliminary gravity results from Zambia (I. M. Cowan and H. N. Pollack, personal communication, 1975) both support the existence of this tectonic trend. Persuasive evidence for contemporary tectonism can be found in the level of seismic activity and the delineation of

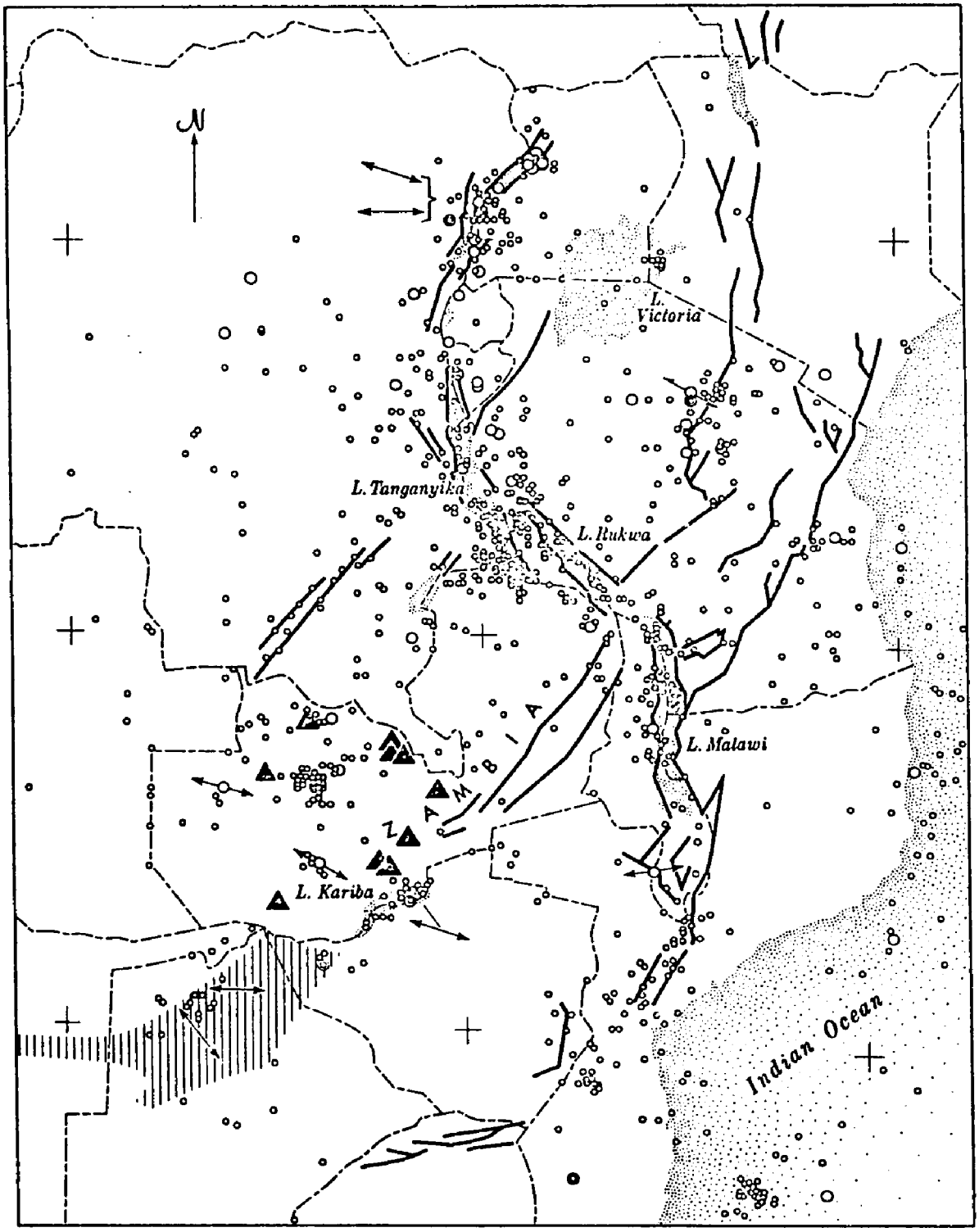



Figure 1. Tectonics of East and Central Africa. Bold lines represent faults, small circles (3 ≤ magnitude < 5) and large circles (5 ≤ magnitude) show earthquake epicenters for the period 1965 to 1970, arrows indicate tensional axis for earthquake source mechanisms, shaded region locates electrical conductivity anomaly. Triangles locate Zambian heat flow sites.

seismic zones in the Central African plateau, which indicate that the region is undergoing substantial tectonic stress release.

To these observations I now add evidence of a broad anomalous heat-flow zone in west and central Zambia, where the heat-flow values are anomalously high by some 50% in comparison to those of contemporary tectonic provinces elsewhere. The anomaly persists after deducting the radioactivity of surface rocks and therefore must be due to some deeper source. The interpretation given to this thermal anomaly lends support to the hypothesis of incipient rifting in the Central African plateau.

# CHAPTER II

## GEOTHERMAL MEASUREMENTS AND DATA REDUCTION

The vertical component of heat flow is calculated from the fundamental relation $q = k(\partial T/\partial z)$ where k is the thermal conductivity of the rock, and $(\partial T/\partial z)$ the vertical temperature gradient. The temperature gradient is determined experimentally in the field by making temperature measurements in deep drill holes or mines, whereas the thermal conductivity is usually determined in the laboratory. In this chapter, the equipment and experimental procedure utilized in making temperature and conductivity measurements are described and results are presented. Results of radioactive heat production of representative rocks are also given.

### Temperature

Temperatures in boreholes were measured with a thermistor probe in combination with a Wheatstone type resistance bridge. Details of the thermistor probe construction and the measuring circuit are given in Appendix I. The equipment was designed to optimize performance standards of sensitivity (± 0.002 K), high power dissipation (50 mW $K^{-1}$ in still water), fast response time (approximately 5 s to 63% change), ruggedness and portability. The bridges and probes have been operated in conditions ranging from the deserts of Niger to the humid underground environment of the copper mines in Zambia without serious mechanical or electrical difficulty.

All probes were calibrated against a Hewlett Packard HP 2850 Series quartz thermometer, whose own calibration is traceable to the National Bureau of Standards. Calibration points at approximately 10 K intervals over the range $0^{o}C$ to $60^{o}C$ were used to determine a single curve of the form

$$R = \exp\left(A + \frac{B}{T + C}\right)$$

for each probe, where R is the resistance at temperature T, and A, B and C are calibration constants. Individual calibration constants are given in Appendix I. The constants were used to construct tables of temperature for resistance increments of 1 ohm, equivalent to temperature increments of about 0.002 K.

Temperature uncertainties arise from (1) calibration errors, (2) thermistor instability, (3) measurement uncertainties and (4) the lack of precise reproducibility in the field. These factors are discussed separately in Appendix I. The overall uncertainty in relative temperatures measured with a single probe is about 0.01 K, whereas the absolute accuracy is 0.1 K.

During field operation, temperatures were measured at discrete intervals, usually 10 m, by making electrical connections through the reel when the cable was stationary. Standard procedure was to allow about five minutes for the probe to equilibrate with its surroundings before obtaining a temperature reading.

Between 1970 and 1974, temperature surveys were conducted in 58 boreholes which had been drilled by mining companies and the Geological Survey of Zambia. Another 108 boreholes which had been drilled to at least 150 m depth were located but were found to be plugged within 100 m

of the surface, rendering the hole useless for heat-flow purposes. In 1973 a program of delivering rigid thin wall plastic pipe to the drill sites for insertion in new drill holes prior to retracting the drill casing was initiated. Three new heat-flow sites resulted from this innovation.

Of the 58 temperature surveys conducted, 23 surveys at 11 separate sites yielded relatively undisturbed geothermal gradients. Complete details for these boreholes, including site location and elevation, drilling and survey histories, inclination of drill hole, temperature-depth values and summary geologic log are given in Appendix II. Temperature-depth curves for 17 of the boreholes at 8 sites are shown in Figure 2. Solid lines have been fitted to the data only for those sections of the boreholes used to calculate heat flow.

The topography at most of the sites is extremely flat, amounting to, in most cases, a few tens of meters change in elevation over several kilometers horizontally. The topographic correction (Birch, 1950) to the temperature gradient for borehole MH 43, the site with the greatest topographic relief, amounts to only 3%, and therefore such corrections can be safely neglected. No corrections to the temperature gradients for possible climatic change have been applied as their effects are considered to be small and the climatic history uncertain. The geothermal gradients for the boreholes in Figure 2 range from 18.8 K $km^{-1}$ in COL 2 to 25.4 K $km^{-1}$ in LUB 1, with a mean and standard deviation of 22.8 and 1.9 K $km^{-1}$ respectively. The mean and standard deviation of the entire set of 23 geothermal gradients determined in this study are 21.9 and 2.9 K $km^{-1}$. Individual measurements will be discussed in a subsequent section on heat flow, but collectively these results comprise a set of

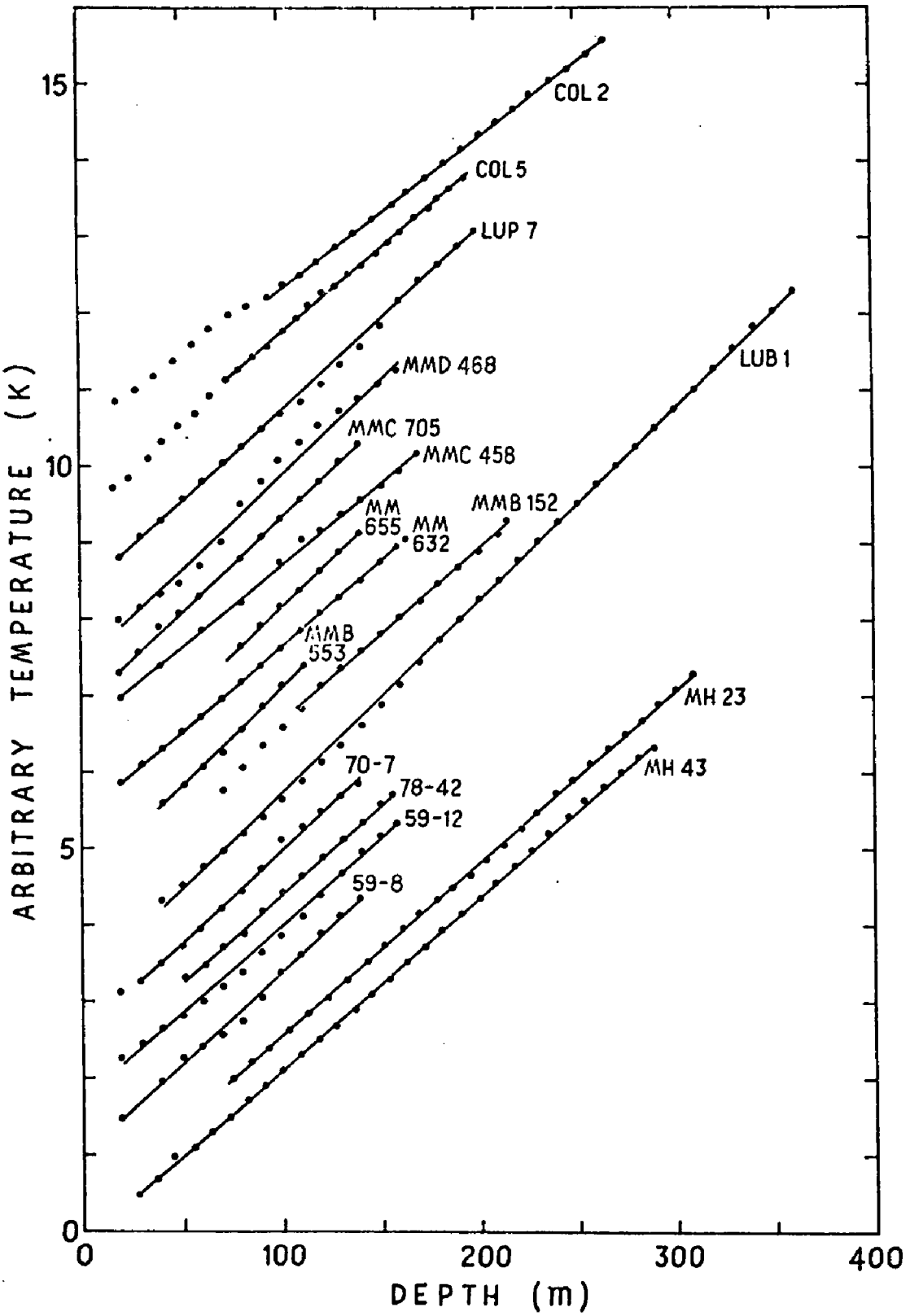



Figure 2. Temperature-depth curves at selected heat flow sites. Borehole code and sites include: COL, Mkushi; LUP, Lumpuma; MMD, Lubwe; MMC and MM, Chimiwungo; MMB, Malundwe; LUB, Lubombo; 70-7 etc., Chalalobuka; MH Munali Hills.

geotherms that are higher than normal for Precambrian terrains and remarkably uniform for sites distributed over a region of several hundred kilometers dimension.

## Thermal Conductivity

All thermal conductivity measurements were made with a variant of the divided bar method (Birch, 1950) described in detail in Appendix I. Cylindrical rock specimens of unknown conductivity were placed in series with reference glass discs and copper discs containing wells for temperature transducers. The extreme ends of the stack were held at different, constant temperatures, and when the stack had achieved a thermal steady state, the temperature drops across the glass reference discs and the sample discs were recorded. The sample conductivity relative to that of fused silica is determined from the ratios of the temperature drops and the thickness of the sample (see Appendix I).

All samples were in the form of circular discs with uniformly prepared flat parallel faces, the diameter depending on the diameter of the drill core. The faces were ground flat and parallel within tolerances of 0.025 mm and 0.08 mm respectively. When coated with a film of liquid detergent and loaded with a constant axial stress, these surfaces provide low-contact resistances, typically 3% of the sample thermal resistance. All rocks were saturated with water prior to measurement by placing them in an evacuated vessel for several hours and then allowing water to enter the vessel under vacuum.

Reproducibility of thermal conductivity determinations is typically better than 2%. One sample, DS4 75m, has been measured on 7 separate occasions: none of the determinations has differed from the mean value

of 3.06 W $m^{-1}$ $K^{-1}$ by more than 1%, and the average deviation from the mean is only 0.2%. Such uncertainties are acceptable, as real fluctuations of conductivity, even in apparently homogeneous samples, commonly amount to 10% or more.

The absolute value of thermal conductivity depends on the Ratcliffe (1959) formulas for fused silica, which, when compared with other determinations for quartz and silica glass (see discussion in Roy et al., 1969), show consistency to within a few percent.

The possibility of having systematic errors arising from the adopted values for the Michigan set of standards or the methodology described in this study was tested by exchanging rock discs with three established geothermal laboratories: Earth Physics Branch, Ottawa; United States Geological Survey, Menlo Park; and Southern Methodist University. The comparison set of samples consisted of thirteen discs of mixed diameter and a wide conductivity range from 1.75 to 4.86 W $m^{-1}$ $K^{-1}$. No attempt was made to standardize the measurement or data reduction procedures. Therefore the results will indicate the total variability between laboratories but will not reveal whether the differences arise from adopted values of standards, calibration procedures, contact resistance problems, diameter mismatch corrections or other possible factors. Such a gross comparison is useful as it is the total conductivity value arrived at under normal operating conditions in a particular laboratory which is used in the computation of heat-flow values. The comparative results are shown graphically in Figure 3. No serious systematic discrepancies are evident in the results from any of the four laboratories. The Michigan results have an arithmetic and rms deviation from the mean of -0.8% and 2.5% respectively for the

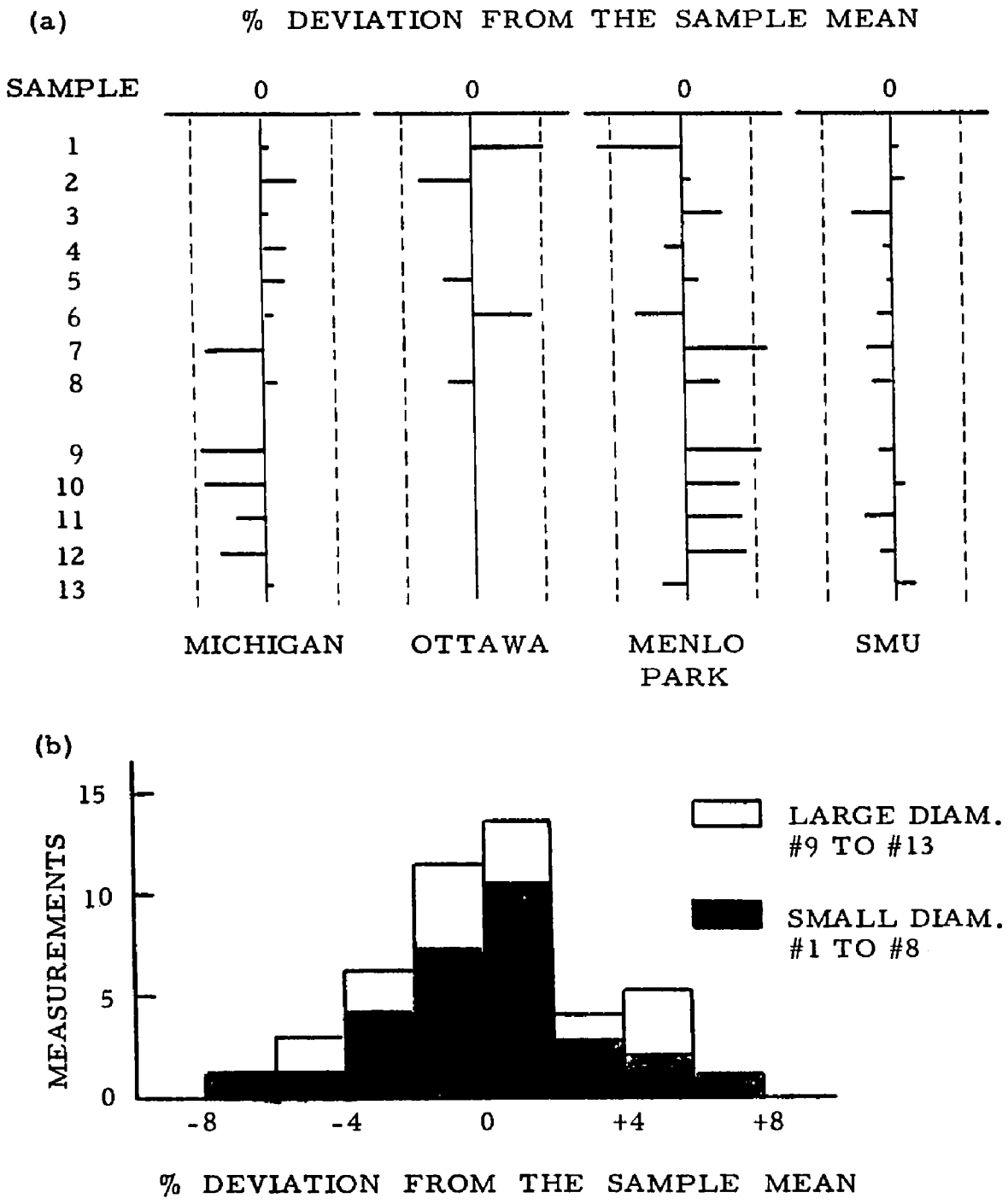



Figure 3. Comparison of thermal conductivity values for rock samples measured at four geothermal laboratories. (a) Individual results for 13 samples; dashed lines show 5% deviation from sample mean. (b) Composite result for all laboratories; rms deviation from the sample mean is 2.8%.

entire collection, values which approach the probable experimental uncertainty.

## Heat Flow

The vertical component of heat flow q is obtained by taking the product of the measured thermal conductivity k and vertical temperature gradient ($\partial T/\partial z$) according to $q = k(\partial T/\partial z)$. All heat-flow values reported in this study were calculated as the product of the harmonic mean conductivity (i.e., reciprocal of mean resistivity) and the least-squares fitted temperature gradient applied to the entire undisturbed section of the borehole.

The possibility of systematic variation of heat flow with depth was checked by the 'interval method' in which heat flow is calculated for sequential 30 m intervals of depth throughout the entire borehole. A second consistency check was provided by computing the summed thermal resistance after Bullard (1939). As

$$T = T_0 + q \sum \frac{1}{k} dz$$

the value of q is found as the slope of the least-squares line of T versus the resistance sum $\sum \frac{dz}{k}$. Systematic variation of heat flow with depth or disturbing effects such as water flow will be indicated by departures from a straight line.

The major result from checking with both the interval and Bullard methods was that the upper sections of several boreholes were discarded since the apparent heat flow either fluctuated widely or departed significantly from the more consistent results from deeper sections. For the depth ranges finally used in heat-flow calculations (see Table 1)

TABLE 1

Zambia Heat Flow Data

| Locality | Latitude | Longitude | Elevation (m) | Depth Range (m) | N | k ($Wm^{-1}K^{-1}$) | $\frac{dT}{dz}$ ($mKm^{-1}$) | q ($mWm^{-2}$) |
|---|---|---|---|---|---|---|---|---|
| Lumwana[1] | 12°15'S | 25°51'E | | | | | | mean 57 |
| Malundwe | 12°14'S | 25°49'E | 1290 ± 10 | | | | | mean 62 |
| MMB 152 | | | | 120- 208 | 19 | 2.65 | 21.4 | 57 ± 8 |
| MMB 553 | | | | 40- 113 | 11 | 2.76 | 24.9 | 69 ± 6 |
| Chimiwungo | 12°17'S | 25°53'E | 1350 ± 10 | | | | | mean 55 |
| MM 632 | | | | 20- 163 | 13 | 2.43 | 22.1 | 54 ± 6 |
| MM 655 | | | | 60- 140 | 9 | 2.16 | 24.0 | 52 ± 6 |
| MMC 458 | | | | 20- 175 | 19 | 2.17 | 20.5 | 45 ± 4 |
| MMC 705 | | | | 20- 140 | 12 | 2.70 | 24.7 | 67 ± 7 |
| Lubwe | 12°10'S | 25°57'E | 1356 ± 10 | | | | | mean 54 |
| MMD 468 | | | | 20- 176 | 18 | 2.21 | 24.5 | 54 ± 6 |
| Ichimpe | 12°44'S | 28°07'E | 1210 ± 15 | | | | | mean 74 |
| PE 2 | | | | 20- 500 | 11 | 3.89 | 19.0 | 74 ± 5 |
| Lumpuma | 13°05'S | 28°03'E | 1204 ± 30 | | | | | mean 65 |
| LUP 7 | | | | 20- 198 | 19 | 2.73 | 23.6 | 65 ± 4 |
| Luanshya Mine | 13°05'S | 28°19'E | 1256 ± 10 | | | | | mean 76 |
| 28 Shaft[2] | | | | 0-1150 | 45 | 3.30 | 23.1 | 76 ± 4 |
| P 38 | | | | 960-1150 | 27 | 3.30 | 19.8 | 65 ± 6 |
| BX 168 | | | | 395- 575 | 7 | 4.28 | 17.8 | 76 ± 5 |
| DH 3465 | | | | 680- 994 | 15 | 4.05 | 20.0 | 81 ± 5 |
| DH 2231 | | | | 681- 852 | 20 | 3.07 | 18.0 | 55 ± 8 |
| Mkushi | 13°55'S | 29°12'E | 1125 ± 15 | | | | | mean 61 |
| COL 2 | | | | 114- 279 | 20 | 3.24 | 18.8 | 61 ± 2 |
| COL 5 | | | | 64- 201 | 16 | 2.98 | 20.5 | 61 ± 3 |

TABLE 1.--Continued

Zambia Heat Flow Data

| Locality | Latitude | Longitude | Elevation (m) | Depth Range (m) | N | k ($Wm^{-1}K^{-1}$) | $\frac{dT}{dz}$ ($mKm^{-1}$) | q ($MWm^{-2}$) |
|---|---|---|---|---|---|---|---|---|
| Chalalobuka | 15°13'S | 28°33'E | 1110 ± 15 | 112- 279 | | | | mean 66 |
| CH 78-42 | | | | 50- 161 | 11 | 2.90 | 22.0 | 64 ± 7 |
| CH 70-7 | | | | 30- | 16 | 3.12 | 23.0 | 72 ± 7 |
| CH 59-12 | | | | 20- 164 | 13 | 3.11 | 21.9 | 68 ± 4 |
| CH 59-8 | | | | 20- 150 | 7 | 2.63 | 23.3 | 61 ± 6 |
| Munali Hills | 15°55'S | 28°08'E | 1097 ± 15 | | | | | mean 64 |
| MH 23 | | | | 70- 309 | 7 | 2.82 | 22.6 | 64 ± 3 |
| MG 43 | | | | 27- 290 | | 2.82[3] | 22.6 | 64 ± 3 |
| Lubombo | 15°49'S | 27°55'E | 1009 ± 3 | | | | | mean 71 |
| LUB 1 | | | | 40- 360 | 10 | 2.81 | 25.4 | 71 ± 3 |
| Machili | 16°52'S | 25°08'S | 1095 ± 10 | | | | | mean 67 |
| GS 108 | | | | 164- 302 | 13 | 3.00 | 22.3 | 67 ± 11 |

Footnotes to Table 1:
[1]Lumwana is a regional name for the collection of sites Malundwe, Chimiwungo, and Lubwe.

[2]Temperatures obtained on seven levels.

[3]Conductivity mean taken from MH 23 samples.

Definitions: N, number of conductivity samples; k, harmonic mean thermal conductivity; dT/dz, least squares temperature gradient; q, heat flow.

the value in the table agrees with the mean interval heat flow and the resistance integral heat flow to within 5% in all cases.

Bullard plots of temperature versus the thermal resistance sum are shown in Figure 4 for the undisturbed sections of selected boreholes. The zero depth in the resistance sum corresponds to the minimum value in the depth range column in Table 1. Bullard plot gradients equal to heat-flow values between 0 and 100 mW $m^{-2}$ are included in Figure 4 for comparison. It is clear that most of the Zambian heat-flow values lie between 60 and 80 mW $m^{-2}$. Also the uncertainty in the slope of a line fitted to the data appears to be considerably less than 10% for most boreholes.

Heat-flow results calculated directly from the gradient and mean conductivity values for 22 boreholes and one mine shaft at 11 distinct sites are presented in Table 1. For each borehole the depth range used for calculating heat flow, the number of conductivity samples, the harmonic mean conductivity, and the least-squares temperature gradient is given in addition to the heat-flow value. For a formal estimate of the reliability of an individual heat-flow value, it is customary (Roy et al., 1969; Sass et al., 1971) to include some statistical measure of the combined scatter in geothermal gradient and thermal conductivity data. The reliability index used in this study, and included as individual heat-flow uncertainty in Table 1, is the standard error of the mean heat-flow in a borehole. Twice this value corresponds to the 95% confidence level for the mean, and in the absence of systematic disturbances caused by uneven topography, uplift and erosion, recent climatic change, or water circulation, should characterize the scatter among component heat-flow values at a single site. Only two heat-flow values fall more

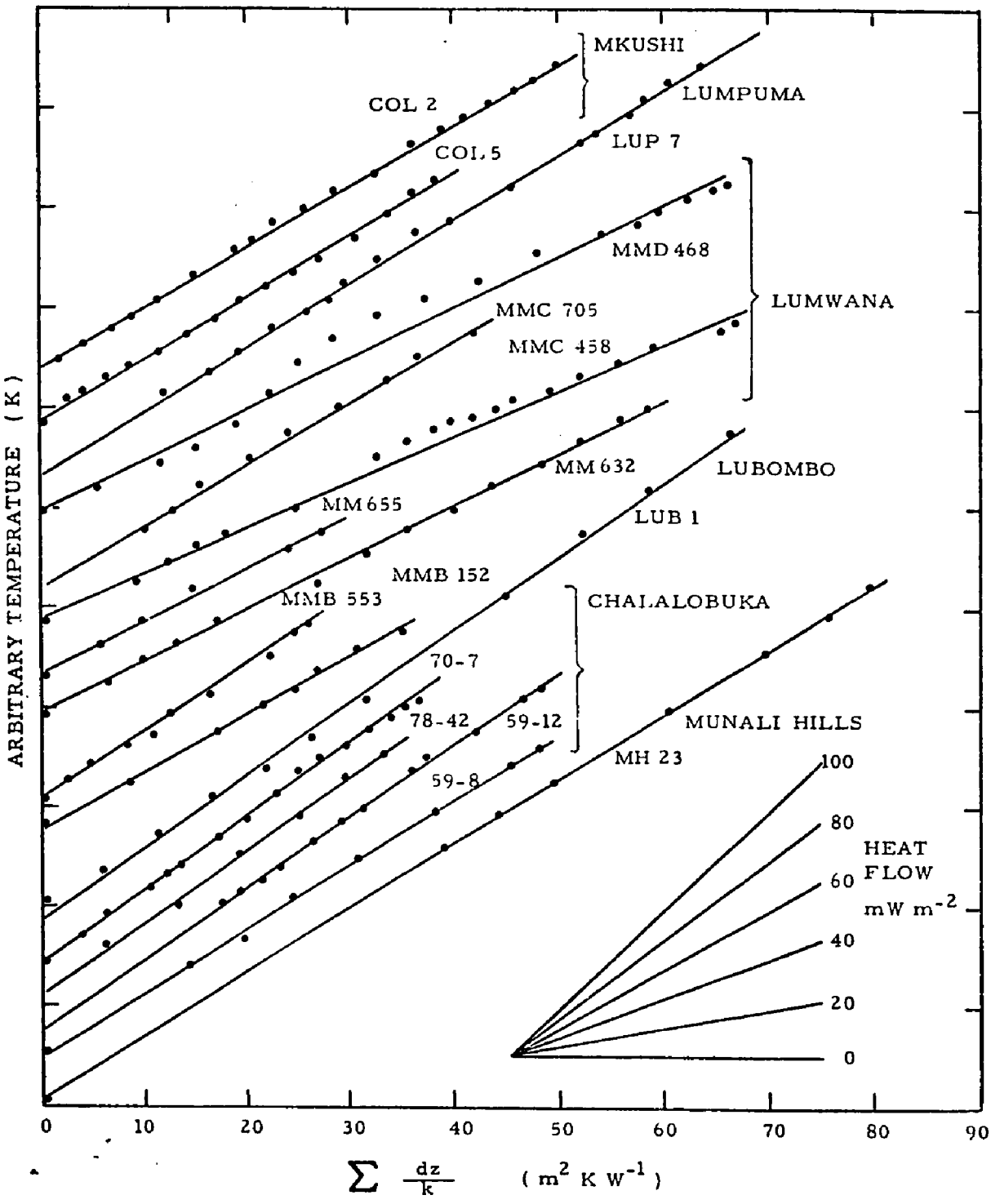



Figure 4. Bullard plot of temperature versus summed thermal resistance for a selection of boreholes. The gradient of each curve yields a heat flow.

than two standard errors from their respective site means.

Where several boreholes lie within a 10 $km^2$ area, a site mean has been calculated for those boreholes, weighted by the reciprocal of the standard deviation in the individual borehole heat-flow value (Beers, 1962, p. 37). Heat-flow results for individual boreholes range between 45 and 81 mW $m^{-2}$, whereas the site means vary only from 54 to 76 mW $m^{-2}$.

Before these heat-flow results are considered in terms of the tectonic setting and in relation to heat-generation results, the geology of each site will be discussed. The general geochronology of Central Africa and the relative positions of lithostratigraphic units to be mentioned in subsequent discussions are summarized in Table 2.

Mkushi

The rocks of the Mkushi site area are biotite gneisses of Precambrian age, considered by Stillman (1965) to have been derived from an ancient pre-Tumbide basement of granite and granite-gneiss by shearing and crushing during the Tumbide (1800 Myr.) orogeny. The gneisses are normally fine grained and well foliated, but are extensively granitized in places and can be coarsely porphyroblastic. The dominant, and often the only visible structure is a well developed north-northeast to northeast-striking foliation, parallel to conformal outliers of Kalonga metasediments to the north of the area. The two boreholes, sited 100 m apart, intersect biotite gneisses and a range of lensoid acid intrusive bodies from pegmatites through granites to aplite, some of them carrying copper mineralization. A typical aplite from the Munshiwemba section, 4 km southeast of the drillholes has been dated at 1625 ± 25 Myr. (Snelling et al., 1964). Both boreholes yield identical heat flow

TABLE 2

Geochronology and Lithostratigraphic Classification
for Central Africa

| Orogeny | Lithostratigraphic Subdivision | |
|---|---|---|
| | Karroo System (Permian - Jurassic) | |
| Pan-African: 450-680 Myr<br>Damaran episode (younger)<br>Lufilian or Katangan episode (older) | | |
| | Katangan System<br>Kundulungu Series<br>Mine Series | Kafue Rhyolite Formation (possibly older) |
| (all pre-Katanga units are grouped as Basement Complex) | | |
| Kibaran: 1300 ± 40 Myr<br>Irumide episode (younger)<br>Tumbide episode (older) | | |
| | | Kalonga Formation |
| | Muva System | |
| | Lufubu System | |
| | | Mkushi Gneiss Formation |

Geological units are listed in chronological order from youngest to oldest, although correlation between units from different areas is very uncertain.

Sources: De Swardt and Drysdall, 1964; Cahen and Snelling, 1966; Clifford, 1968; Drysdall, et al., 1972.

values of 61 ± 3 mW $m^{-2}$ in spite of the differences in temperature gradients, thus providing a good example of the sympathetic variation of geothermal gradient and local thermal conductivity.

Chalalobuka

The Chalalobuka heat flow site is north of the Chongwe River in foliated granite gneisses belonging to the Gneiss Group of the Basement Complex (Garrard, 1968). General northwest-striking folds have resulted from a primary phase of the Lufilian orogeny (c. 730 Myr. in central and southern Zambia, Snelling et al., 1972). Boreholes there were drilled to intersect copper mineralization associated with a layer of quartz-biotite-garnet schist which dips approximately 17° to the south. Boreholes 59-8, 59-12 and 70-7 are clustered together within a 60 m radius and separated from borehole 78-42 which lies 600 m to the southeast. In spite of the shallow depths (less than 164 m) all four holes yield consistent heat flow values between 61 ± 6 and 72 ± 7 mW $m^{-2}$.

Munali Hills and Lubombo

Munali Hills and Lubombo heat-flow sites may be grouped together in a general geological discussion of the Kafue and Mazabuka areas. Older Precambrian metamorphic sequences including the Mpande gneiss and Kafue rhyolite are uncomformably overlain by metasediments and metavolcanics. The sites lie west of the Munali Hills within a metasedimentary succession described as the Mazabuka Group (Smith, 1963) which may be of either Katangan age or considerably older (de Swardt and Simpson, 1972). Thermal overprinting in the area is recorded by two groups of radiometric ages 425-562 Myr. and around 730 Myr. (Snelling et al., 1972) related to the Lufilian orogeny.

Both Munali Hills boreholes were inclined to intersect a northwest-striking tabular gabbro body, about 500 m thick, which dips at 70° to the southwest. Borehole MH 23 is collared in quartzite to the southwest of the buried gabbro outcrop and penetrates the gabbro for the lowermost 230 m of the hole. MH 43 is collared 1.6 km to the west of MH 23 within the buried outcrop and penetrates gabbro for the entire drillhole. Solid-disc conductivity samples were unavailable for MH 43; instead, the average conductivity value for the gabbro in MH 23 was used in computing the MH 43 heat flow. Identical heat-flow values of 64 ± 3 mW $m^{-2}$ result for both Munali Hills holes. Borehole LUB 1 was drilled 25 km to the northwest of Munali Hills, along strike of the general structure, and penetrates mainly feldspathic gneiss and a series of coarse granite and gabbro layers in the lower section of the hole. The computed heat-flow value of 71 ± 3 mW $m^{-2}$ is consistent with the values from Munali Hills.

## Lumwana Region

Lumwana is the regional name used for the collection of sites (Malundwe, Chimiwungo, and Lubwe) which lie respectively on the southwest, south, and eastern edges of the Mombeshi Dome. The central part of the dome is flanked by Precambrian basement schist and paragneiss rocks and inliers of Katangan age schists, in and around which much of the exploration drilling has taken place.

## Malundwe

The heat flow at Malundwe is based on two vertical holes MMB 152 and MMB 553 situated 800 m apart. The very steep gradient in the uppermost 120 m of MMB 152 probably results from subnormal soil temperatures in the grassy treeless area (known locally as a dambo) where the borehole

is sited, and has consequently been ignored in the calculation of heat flow. The two Malundwe heat-flow values of 57 ± 8 and 69 ± 6 mW $m^{-2}$ agree within the measurement uncertainties.

Chimiwungo

The four Chimiwungo heat-flow drill sites lie along a north-south gently dipping section, 2.2 km in length. The rocks penetrated are a series of muscovite, kyanite and garnet schists, and pink feldspathic gneiss. The two holes, MM 632 and MM 655, which are south of Kalumazhiba stream yield very similar heat-flow values of 54 ± 6 and 52 ± 6 mW $m^{-2}$, but the spread from 45 ± 4 to 67 ± 7 mW $m^{-2}$ for MMC 458 and MMC 705 is unexplained. Temperature surveys in two other Chimiwungo drillholes MMC 704 and MMC 706, 50 m on either side of MMC 705, were not utilized for further heat-flow determinations but they provided valuable information on the temperature equilibration of drillholes after drilling had ceased. MMC 706 was measured three times at 6, 36, and 54 hours following the completion of drilling, and equilibration temperatures were then predicted using the theory of Lachenbruch and Brewer (1959) (see Chapman et al., 1975 for details). The predicted equilibrium gradient agreed with the observed gradients from MMC 705 and MMC 704 to within 2%, indicating that where boreholes cannot be preserved for subsequent equilibration measurements, a series of non-equilibrium measurements in the period immediately following drilling, and before the drill casing is retracted, will provide acceptable thermal gradient results.

Lubwe

Only a single drillhole MMD 468 was open for measurements. Although the temperatures show some evidence of disturbances, the computed heat

flow of 54 ± 6 mW $m^{-2}$ is consistent with the entire Lumwana region.

Copperbelt Region

The Copperbelt heat flow sites lie within the Lufilian Arc tectonic element, part of an extensive system of African orogenic belts characterized by ages c. 500 Myr (Kennedy, 1965). The Lufilian arc contains folded inliers of late Precambrian sediments of the Katangan system, some intruded granites, and more commonly domes and anticlines of Kibaran age basement. The sedimentation, deformation, and metamorphism of the Katanga system are described by Clifford (1967) and Cahen (1970), and the geochronology is summarized by Snelling, et al. (1972). Fifteen radiometric ages from the Zambian Copperbelt lie within the range 583 ± 90 to 452 ± 24 Myr (Snelling, et al., 1972).

It is unfortunate that the Copperbelt, where mineral exploration boreholes are so numerous, has yielded so few heat-flow sites. The difficulty is not surprising however, as the sedimentary series that contain most of the mineralization are commonly good aquifers as well. Of the 23 surface borehole temperature surveys conducted in the Chililabombwe, Chingola, Kalulushi, Mufulira and Luanshya areas, many to depths of 300 m or more, only three sites proved to be free of major temperature disturbances owing to water flow. These sites are described below.

Luanshya Mine.--Luanshya Mine is in the Roan-Muliashi basin which is a gently plunging synclinal outlier of the Katanga system on the west flank of the Kafue anticline (see inset map, Figure 5). The geology and structure of the explored eastern part of the basin is described in detail by Lee-Potter (1961) and Mendelsohn (1961). A systematic series of temperature measurements to depths of 1200 m was made from under-

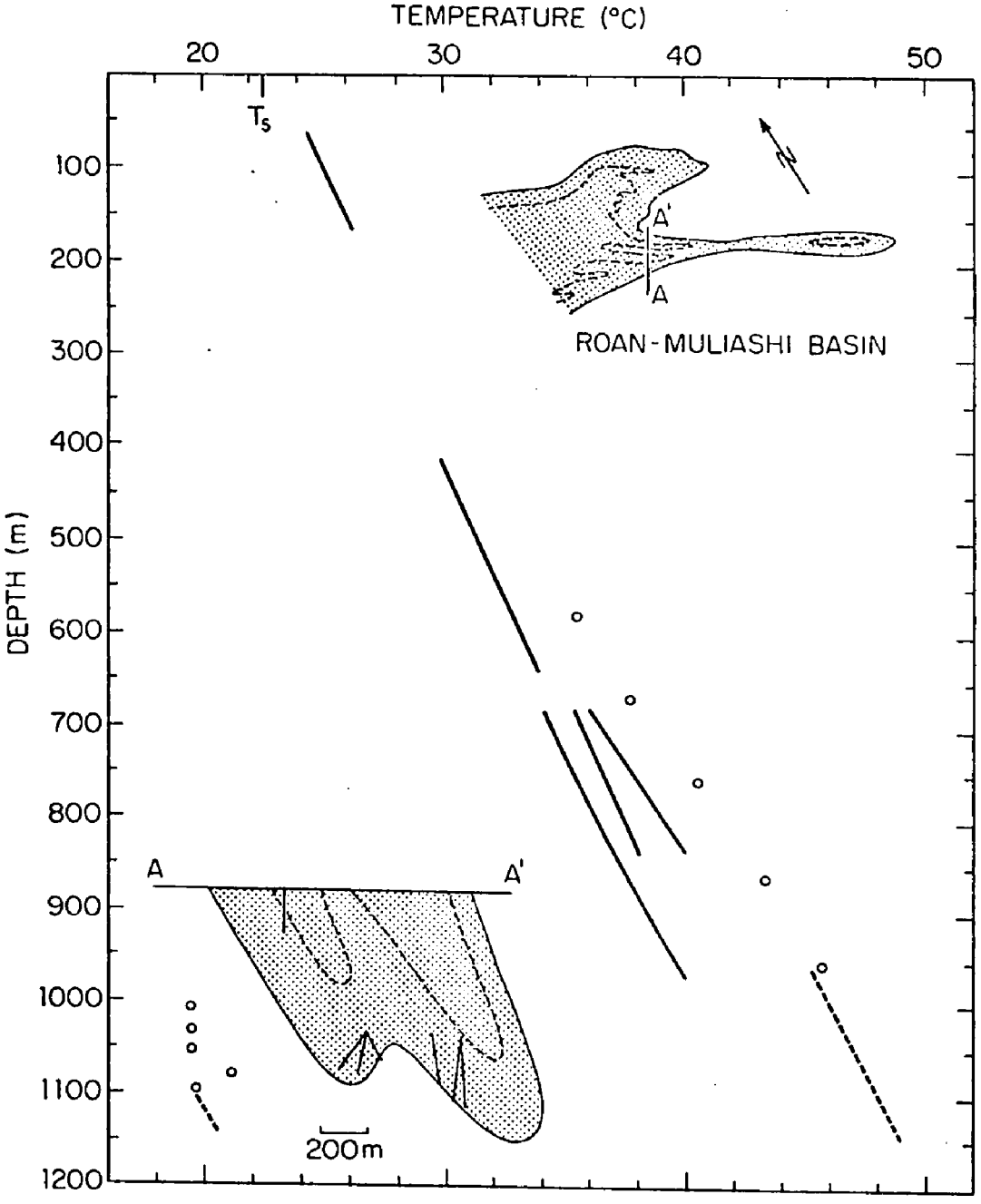



Figure 5. Thermal regime of Luanshya Mine. Insets show location and structure of the Roan-Muliashi Basin containing Mine Series rocks (shaded) surrounded by Basement Complex (unshaded). Most temperature surveys were obtained near section A A' at western boundary of Roan Extension. Open circles and dashed lines represent measurements in Basement Complex; solid lines represent measurements within the syncline.

ground workings both in the Basement Complex adjacent to 28 Shaft (formerly Maclaren Shaft) and in the Mine Series rocks within the syncline. The locations of the surveys, projected along strike to a generalized structure section in Roan Extension, are shown in Figure 5 together with temperature-depth results. Although the average geothermal gradient for the collected results is similar to gradients measured elsewhere in Zambia, there is a significant horizontal temperature gradient within the mine, with temperatures at constant depth decreasing towards the center of the syncline. A further study involving a finite difference heat conduction model of the mine is being undertaken to examine whether thermal conductivity contrasts, or ground water percolation, or both, are likely responsible for this unusual thermal regime. Preliminary heat-flow values, uncorrected for possible structural and geometric effects on the vertical heat flow, have been calculated for four of the underground drill holes as well as for 28 Shaft. Individual values vary between 55 ± 8 and 81 ± 5mW $m^{-2}$ with a weighted mean value of 76 mW $m^{-2}$.

Ichimpe.--Ichimpe is in the Ichimpe forest reserve 10 km north of Kalulushi. Borehole PE 2 penetrates more than 500 m of Katangan siliceous dolomite, locally brecciated. A single temperature survey to a depth of 500 m was conducted at the end of a six day break in the drilling. Although the absolute temperatures obtained so soon after drilling has ceased are unlikely to be equilibrium temperatures, experience has shown that for typical Zambian mineral exploration drilling operations, the temperature gradient obtained a week after drilling ceases is rarely more than a few percent from the equilibrium gradient. The calculated heat flow for Ichimpe is 74 ± 5 mW $m^{-2}$.

Lumpuma.--A single hole LUP 1 was surveyed at Lumpuma, sited 35 km west of Luanshya. The hole penetrates regionally metamorphosed argillaceous sediments and basic intrusive bodies probably belonging to the Muva system with an estimated age of 1200 Myr (Mendelsohn, 1961, p. 18). LUP 1 was surveyed twice, 5 days and then 10 days after drilling had ceased, and, as no perceptible cooling or warming was observed over that period, the gradient obtained was assumed to be close to equilibrium. Subsequently, the hole was again remeasured after a period of 15 months; differences in absolute temperatures at specified depths were nowhere more than $0.07^{o}C$, and the least squares gradients from each of the surveys agreed with one another to within 0.5%. The calculated heat flow for Lumpuma is $65 \pm 4$ mW $m^{-2}$.

Machili

Machili, 10 km southwest of Mulobezi, is the only site in this study which is in the Karroo age rocks (Permian-Jurassic) of western Zambia. Karroo formations overlie Katangan crystalling rocks in the north and northeast and Basement Complex in the southeast. Borehole GS 108 penetrates a broad fault-bounded Upper Karroo clastic sequence of reddish sandstones, siltstones and mudstones described in detail by Money (1972). The geothermal gradient for GS 108 decreased steadily from 40 K $km^{-1}$ at 50 m depth to 22 K $km^{-1}$ at 164 m although the thermal conductivity remains virtually constant over the same interval. A heat-flow value of $67 \pm 11$ mW $m^{-2}$ has been computed for the depth interval 164 to 302 m where the gradient is quite linear, but the disturbance in the upper section of the borehole makes this result rather uncertain.

## Heat Production

The radioactive heat generation of representative rocks from the heat flow sites was determined by gamma ray spectroscopy methods in the rock radiometry laboratory at Purdue University. Measurements were normally made on 1 kg aggregate crushed specimens comprising several individual samples collected at regular intervals along the drill core. Measurement uncertainties were reduced to 2% by employing appropriately long counting times. Uncertainty due to sampling bias is more difficult to estimate, but it is believed to be limited to about 15% by the use of the composite sample. Detailed results of fourteen heat production determinations from the heat flow sites are given in Table 3. For each determination, the site or drill hole, the number of samples in the composite, predominant rock type, the U, Th, and K concentrations and computed heat generation are given. Heat-production values were calculated from the measured abundances of uranium, thorium, and potassium using the relation (after Birch, 1954, Chapter 5)

$$A = 0.01\ \rho\ (9.69\ U + 2.65\ Th + 3.58\ K)$$

where A is heat production in $\mu W m^{-3}$, $\rho$ is density in g $cm^{-3}$, U is uranium concentration in ppm, Th is thorium concentration in ppm, and K is potassium content in percent.

The majority of the samples consist of granite gneisses, biotite gneisses, mica schists and amphibolites belonging to the pre-Katanga basement and Katanga metasediments (De Swardt and Drysdall, 1964). In some cases the aggregate samples from the borehole drill core typify the regional petrology of the site for several kilometers around and are used directly for the site mean value. In other cases the boreholes

TABLE 3

Heat-Production Results from Heat-Flow Sites

| Site | N | Depth Range (m) | Rock Type | U (ppm) | Th (ppm) | K (%) | A ($\mu W\ m^{-3}$) |
|---|---|---|---|---|---|---|---|
| Mkushi | | | | | | | mean 1.9 |
| COL 2 | 25 | 52-310 | granitic & biotitic gneiss | 4.1 | 6.2 | 3.3 | 1.8 |
| COL 5a | 15 | 23-145 | granitic & biotitic gneiss | 3.7 | 9.0 | 2.9 | 1.9 |
| COL 5b | 11 | 158-270 | granitic & biotitic gneiss | 3.7 | 8.8 | 3.3 | 1.9 |
| Chalalobuka | | | | | | | mean 2.3 |
| CHAL 11 | 22 | 41-165 | biotite & amphibolite schists, | 5.4 | 8.7 | 2.7 | 2.3 |
| Lubombo | | | | | | | mean 3.6 |
| LUB 1a | 1 | 248 | granite | 6.8 | 13.2 | 4.7 | 3.2 |
| LUB 1b | 10 | 43-185 | biotite schist | 3.4 | 17.4 | 3.4 | 2.4 |
| LUB 1c | 13 | 205-382 | granite, amphibolite | 7.7 | 40.3 | 4.0 | 5.2 |
| Lumwana | | | | | | | mean 2.5 |
| LUMW 1[2] | 10 | 31-162 | mica schists | 4.5 | 13.2 | 3.7 | 2.5 |
| Lumpuma | | | | | | | mean 1.8* |
| LUP 7a | 7 | 30-134 | garnet mica schists | 1.6 | 15.3 | 2.7 | 1.8 |
| LUP 7b | 8 | 15-195 | gabbro | 1.4 | 7.6 | 1.9 | 1.1 |
| Munali Hills | | | | | | | mean 2.4* |
| MH 23a | 10 | 18-108 | quartzite, schists | 1.5 | 5.7 | 1.5 | 0.94 |
| MH 23b | 13 | 124-324 | gabbro | 0.3 | 0.9 | 0.3 | 0.16 |
| MH 43a | 8 | 45-162 | gabbro | 0.3 | 0.8 | 0.3 | 0.16 |
| MH 43b | 8 | 178-296 | gabbro | 0.6 | 1.6 | 0.3 | 0.29 |

[1]Samples from boreholes CH 70-7, CH 59-12, CH 59-8.

[2]Samples from boreholes MMB 152, MMB 553, MMD 468, MMC 705, MMC 458.

*See text for discussion.

penetrate rock that is very localized in vertical and horizontal extent, and in such cases the site mean is weighted by the regional extent of certain rock types. The subjective nature of such a weighting procedure is recognized, and therefore estimations of maximum heat production are made so as to minimize any inferred reduced heat-flow anomaly. The affected sites are Lumpuma, where the low value for the localized gabbro which the borehole penetrates has been neglected in computing the site mean, and Munali Hills where the boreholes penetrate a gabbro sill which is also thought to be of limited extent. In the latter site, the value of 2.4 $\mu W\ m^{-3}$ for the biotite schist composite sample at Lubombo 15 km away, which coincides with the mean value for basement rocks elsewhere, is considered to be a more representative value.

In addition to rocks collected at heat flow sites, a small number of specimens was collected from exposed granitic bodies in central and northwestern Zambia specifically for heat-production measurements. These results are given in Table 4. The Solwezi Dome, Nchanga and Hook granite specimens are all highly radioactive owing to unusually high thorium contents (Table 4). For comparison the uranium, thorium and potassium concentrations of the Conway Granite of the White Mountains Plutonic series, often considered a "hot" granite are 15.4 ppm U, 58.7 ppm Th, and 4.1% K, with a heat production value of 8.5 $\mu W\ m^{-3}$. Unfortunately no heat-flow sites are located within these Zambian radioactive bodies.

TABLE 4

Heat Production Results from Granitic Bodies

| Location | N | depth (m) | rock type | U (ppm) | Th (ppm) | K (%) | A ($\mu W\ m^{-3}$) |
|---|---|---|---|---|---|---|---|
| Myombeshi dome | | | | | | | |
| MM 632 | 1 | 100 | pink feldspathic gneiss | 3.7 | 42.4 | 5.6 | 4.5 |
| MM 635 | 1 | 151 | feldspathic augen gneiss | 3.6 | 31.5 | 4.3 | 3.6 |
| Solwezi Dome | | | | | | | |
| Kimali 1 | 1 | 250 | coarse pink granite | 2.1 | 67.2 | 5.1 | 5.8 |
| Kimali 2 | 1 | surface | granite | 4.8 | 51.0 | 4.4 | 5.3 |
| Kimali 3 | 1 | surface | granite | 14.0 | 48.8 | 4.2 | 7.5 |
| Nchanga granite | | | | | | | |
| Chingola 2 | 1 | surface | coarse granite | 12.0 | 65.5 | 4.5 | 8.2 |
| Chingola 7 | 1 | surface | coarse granite | 6.5 | 64.9 | 4.6 | 6.8 |
| Hook granite | | | | | | | |
| Itezhitezhi 3 | 1 | surface | migmatite | 7.3 | 66.9 | 4.5 | 7.1 |
| Itezhitezhi 4 | 1 | surface | pegmatitic granite | 6.5 | 108.5 | 5.4 | 9.9 |
| Itezhitezhi 1 | 1 | surface | feldspar pegmatite | 29.6 | 124.3 | 4.1 | 16.9 |
| Itezhitezhi 2 | 1 | surface | feldspar pegmatite | 17.4 | 117.2 | 4.8 | 13.3 |
| Conway granite* | | | | 15.4 | 58.7 | 4.1 | 8.5 |

*Source: Birch, et al., 1968, Table 33-3.

# CHAPTER III

## INTERPRETATION OF HEAT FLOW AND HEAT PRODUCTION RESULTS

### Tectonic Setting and the Surface Heat Flow Anomaly

Apart from limited areas of Karroo (Permian-Jurassic) sedimentary and volcanic rocks, and Pleistocene Kalahari sands which blanket much of the solid geology in the west, Zambia is underlain mainly by Precambrian rocks. The country can be divided into five principal structural stratigraphic provinces (Drysdall, et al., 1972): (1) the Bangweulu Block in the north, undisturbed since Ubendian (1800 Myr) events; (2) The Kibaran province (1300 ± 40 Myr culmination) comprising a wide variety of granites, gneisses, migmatites, metasediments and metavolcanics making up the pre-Katanga Basement complex in the east and central part of the country; (3) the Katanga system and Lufilian arc lying between the Congo craton to the north and the Kalahari craton to the south, comprising geosynclinal sediments of the Katanga system (1300-620 Myr) deformed principally during the polyphase Lufilian orogeny which is dated in central Zambia at about 720 Myr; (4) the Mozambique belt (c. 460 Myr) in the extreme east and (5) the Karroo basins and troughs which are characteristically fault bounded asymmetrical downwarps partly filled with sub-horizontal, unmetamorphosed continental sediments and locally intercalated basalts. Both the Lufilian arc and the Mozambique belt are considered to be parts of the widespread late Precambrian-early Paleozoic Pan-African orogeny. For

the purpose of subsequent geothermal interpretations, I consider the first four of the above provinces together, separate from the post Pan-African terrain. The distribution of all heat flow sites in relation to this simple tectonic division is shown in Figure 6. Apart from the site at Machili, which penetrates 300 meters of Karroo-age sandstones and mudstones, all the other heat flow stations are in Kibaran or Lufilian tectonic elements. Only at the Kibaran Mkushi site has an older (local) radiometric age of 1635 Myr (Snelling et al., 1964) been determined. The Lufilian heat flow sites probably represent an age spread from 730 ± 50 Myr in the south to 520 ± 50 Myr in the north based on geologic correlation with other areas which have been radiometrically dated.

The tectono-thermal history of heat-flow sites is important because it provides the basis for one of the most important continental heat-flow correlations: that of decreasing heat flow from tectonic elements of increasing age. The most detailed exposition of this relationship is that of Polyak and Smirnov (1968), who divided continental heat flow measurements into subsets corresponding to the age of most recent mobilization. They found the values to be normally distributed about the means of the subset, and the subset means to show a systematic decrease with increasing age (Figure 7). This general relationship has several difficulties when the data are analysed in detail: the age trend does not seem to apply within individual subsets such as Precambrian shields (Rao and Jessop, 1975); and although the subset values are distributed normally in a statistical sense, the low heat-flow values in a subset may have tectonic significance separate from the high values, as for example in the Sierra Nevada Mountains of the Western U.S.A. (Blackwell,

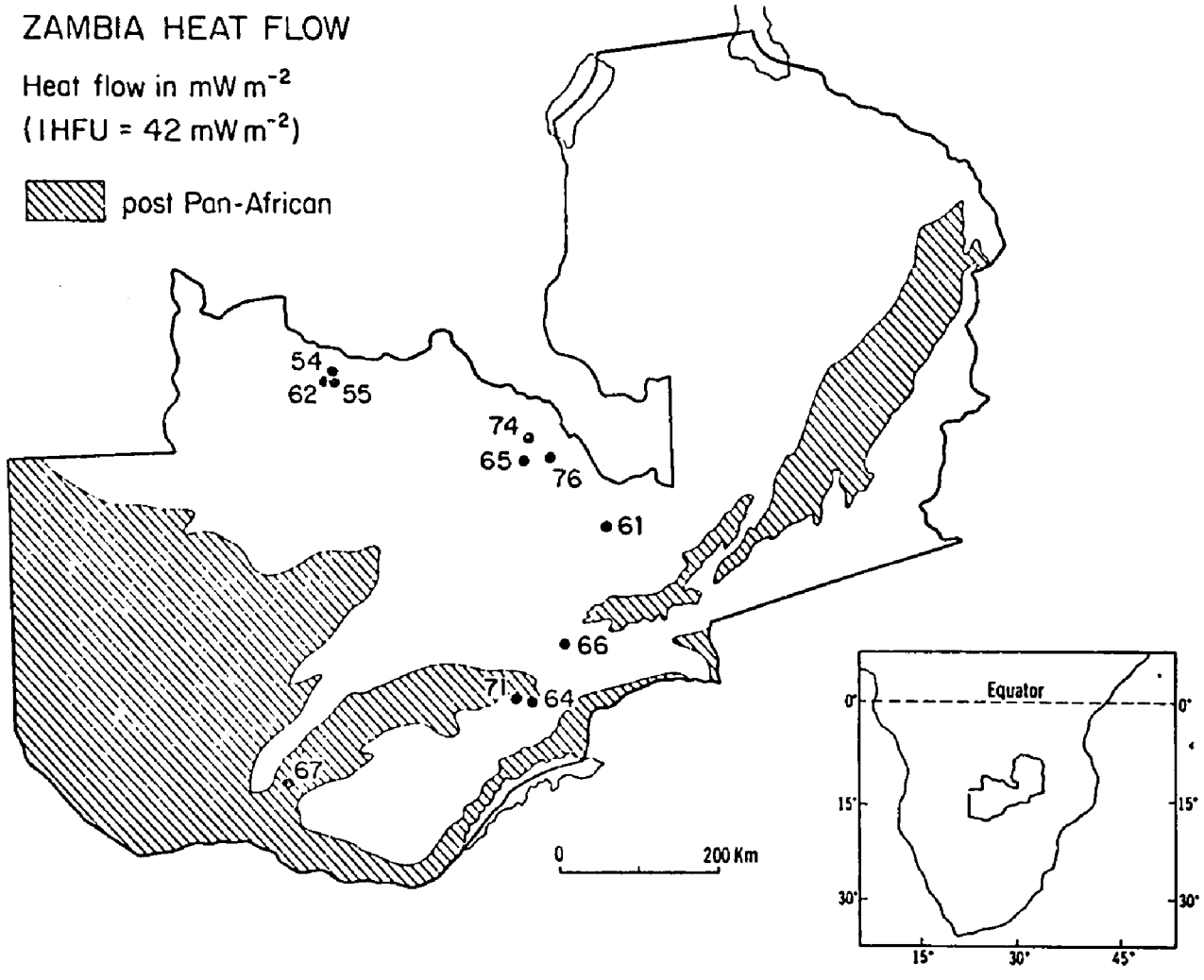



Figure 6. Location map of the Republic of Zambia showing heat flow sites, Precambrian (unshaded) and post Pan-African (shaded) terrains.

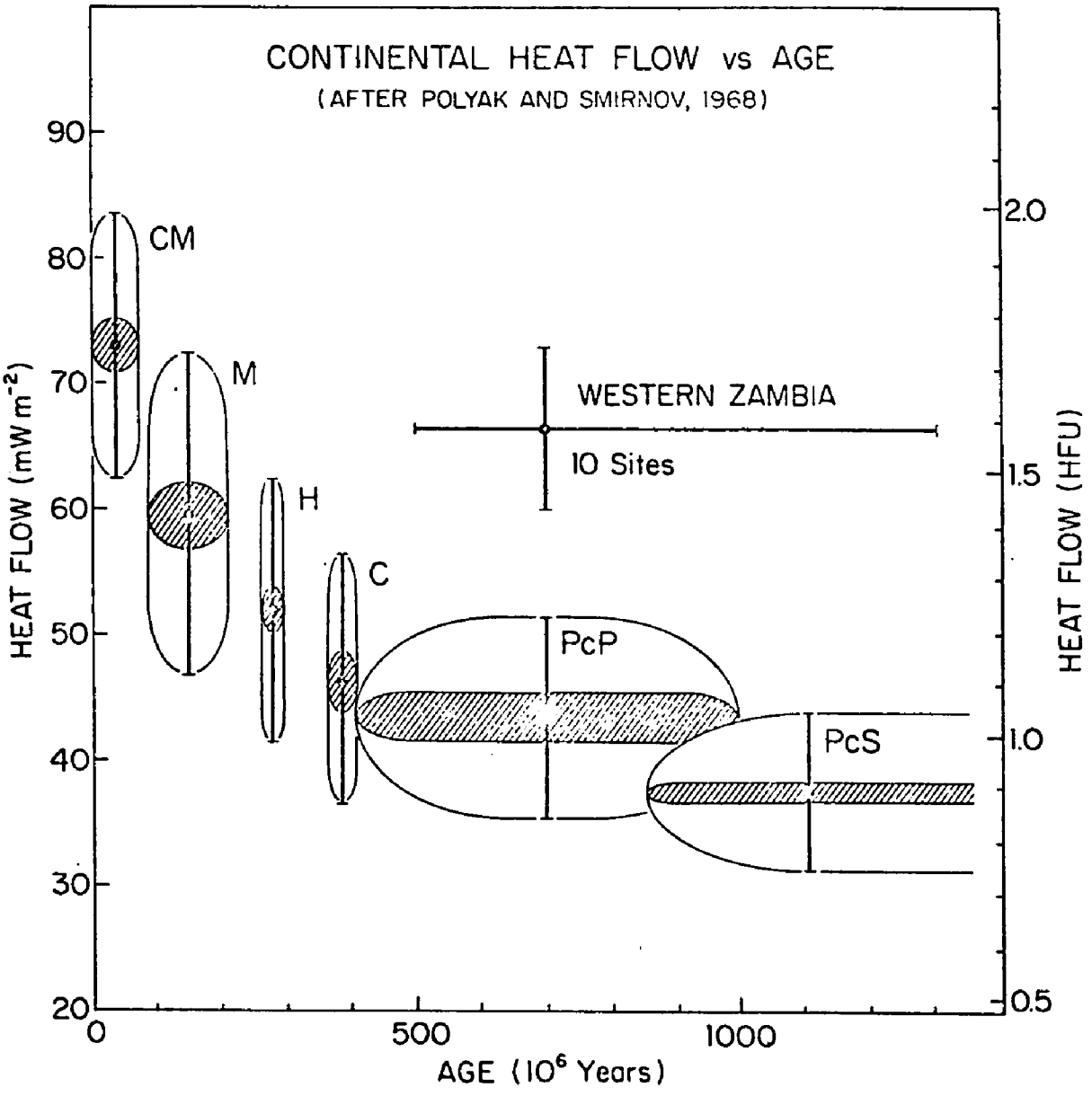



Figure 7. Mean heat flow from the ten Zambian Precambrian sites superimposed on plot of heat flow against age of tectogenesis after Polyak and Smirnov (1968). Tectonic provinces include: PcS, Precambrian shield; PcP, Precambrian platform; C, Caledonian folding; H, Hercynian folding; M, Mesozoic folding; CM, Cenozoic miogeosyncline. Shaded ellipse represents standard error of the mean heat flow; vertical bar and open ellipse represents standard deviation.

1971). In spite of these difficulties, the overall trend seems to be genuine, and it is utilized in the following section.

In Figure 7 the mean value of 66 mW $m^{-2}$ for the 10 Precambrian sites is plotted at a collective representative age of 700 Myr. The standard deviation of the individual heat-flow values and standard error of the mean are 7 and 2.3 mW $m^{-2}$ respectively. It is apparent from Figure 7 that the Zambian surface heat flow is anomalously high, exceeding the mean heat flow for Precambrian shields and platforms by 27 and 22 mW $m^{-2}$ respectively.

Before a tectonic significance is attached to this high heat flow, an estimate must be made of the fraction of the anomaly, if any, that is caused by enhanced heat production in the near-surface rocks. It is therefore appropriate to consider the results of the heat-production measurements.

## Effect of a Radioactive Surface Layer

It is now necessary to estimate what fraction of the apparent surface heat-flow anomaly of about 25 mW $m^{-2}$ (Figure 7) arises from the near surface radiogenic sources and how much has a deeper origin. It is well known that large variations in surface heat flow can arise merely from differences in heat production of a near-surface enriched zone (Roy, et al., 1968b). Furthermore, in order to distinguish geothermal differences between various continental regions, it is desirable to determine the parameters q* and b (the reduced heat flow and characteristic depth of the heat source distribution, respectively), of the empirically determined linear heat flow-heat production relation:

$$q_o = q^* + bA_o$$

where $q_0$ is the surface heat flow and $A_0$ the surface heat production.

Heat flow is plotted against representative heat production in Figure 8 for the six sites where information is available. The good clustering of heat-flow values in this study precludes a meaningful estimation of q* and b by fitting a straight line to the data points. Instead, the non-radiogenic part of the Zambian heat-flow anomaly must be inferred by comparison with results obtained elsewhere. Two types of comparison are considered: the first is a direct comparison of the Zambian heat flow-heat production results with heat flow-heat production trends in other continental regions; the second is a comparison with typical heat-production values alone.

The first comparison may be seen directly in Figure 8. Three previously published lines representing heat flow-heat production relationships have been included: Basin and Range, $q_0 = 59 + 9.4\ A_0$ (Roy et al., 1968); Eastern U.S.A., $q_0 = 34 + 7.5\ A_0$ (Roy et al., 1968); and all shields, $q_0 = 29 + 6.3\ A_0$ (Rao and Jessop, 1975). In these equations, $q_0$, q*, b and $A_0$ have units of mW $m^{-2}$, mW $m^{-2}$, km, and $\mu$W $m^{-3}$, respectively. A fourth line $q_0 = 25 + 11\ A_0$ is included which is a line fit to all published Precambrian heat flow-heat production pairs (Jessop et al., 1975) exclusive of Zambia. The parameters of this line are strongly influenced on the low heat-production end by results from Southern Norway (Swanberg, et al., 1974) and Niger (Chapman and Pollack, 1974) and on the high end by the highly radioactive sites in central Australia (Jaeger, 1970). All the individual Zambian results lie systematically above the curves for the old stable regions, and the departure of the mean heat flow from these lines is between 13 and 20 mW $m^{-2}$ depending on which line is chosen as a reference. This

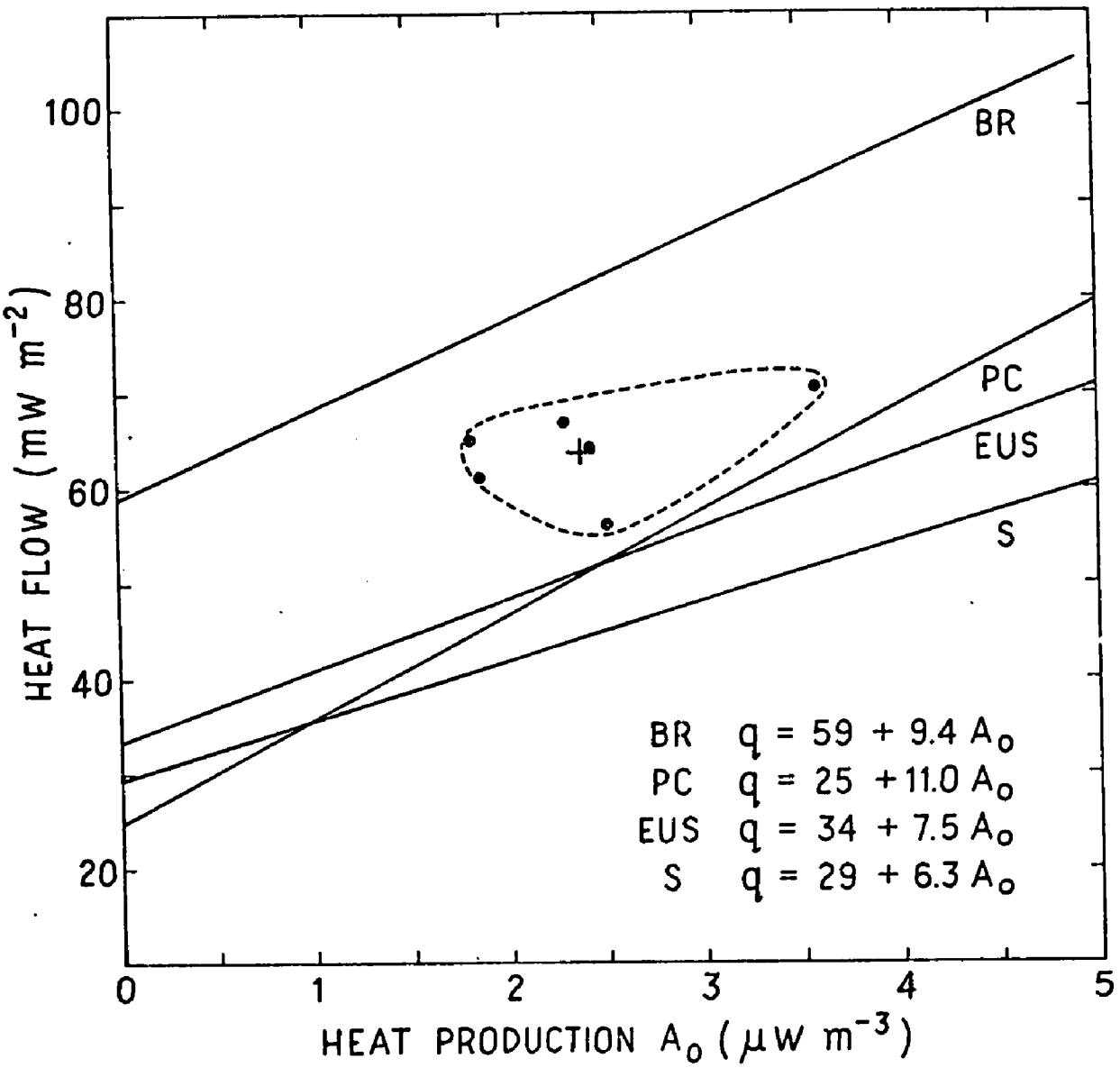



Figure 8. Heat flow and heat production results showing individual site values (•) and the mean value (+) for six Zambian sites. Lines represent published linear heat flow relationships for the following; BR, Basin and Range; PC, all published Precambrian sites; EUS, Eastern United States; S, all shields.

departure is thus an estimate of the residual anomaly not attributable to enhanced near-surface radioactivity. In contrast to the lower three lines in Figure 8, which represent ancient tectonism, the Basin and Range line provides a useful comparison with regions of recent tectonism. The reduced heat flow of 59 mW $m^{-2}$ is considered to be close to the maximum that might be found over broad regions of the continental crust (Blackwell, 1971; Roy, et al., 1972; Diment, et al., 1975).

The alternative method of assessing the non-radiogenic part of the Zambia heat-flow anomaly compares the average abundance of U, Th, and K in large surface areas of old continental regions with the mean heat production value of 2.4 μ W $m^{-3}$ for the Zambian sites. Such a method may avoid biasing from the very restricted distribution in shields of heat flow versus heat production results. Shaw (1967) has estimated 1.6 μ W $m^{-3}$ as a mean heat production for the surficial exposure of the Canadian shield, while Heier and Rogers (1963) obtained 1.7 μ W $m^{-3}$ as a mean for all continental regions. Thus the Zambian terrain appears to have a surface heat-production enhancement $\Delta A_o$ of 0.7 to 0.8 μW $m^{-3}$. The enhanced fraction of the radioactive surface layer in the steady state contributes $\Delta A_o$ b to the surface heat flux independent of the actual vertical distribution, whether it be a stepwise, linear, or exponential decrease with depth. Enhancement values of $\Delta A_o$ = 0.8 μW $m^{-3}$ and b = 11 km, account for only 9 mW $m^{-2}$ of the original 22 to 27 mW $m^{-2}$ surface heat-flow anomaly, leaving a residual anomaly of 13 to 18 mW $m^{-2}$.

Thus, from both of the above comparisons we deduce that enhanced heat production from the surface layer can account for less than half of the Zambian surface heat-flow anomaly, and that a residual heat-flow anomaly of 15 mW $m^{-2}$ or greater persists. It is even less likely that

the anomaly arises from unusual radio-activity at greater depths. The lower crust is thought to consist of granulite facies rocks (see Smithson and Decker, 1974, for discussion) with characteristic heat-production values between 0.2 and 0.5 $\mu W\ m^{-3}$. As this represents a radiogenic depletion by a factor of five to ten relative to upper crustal rocks, it is unlikely that the source of the residual heat flow is radiogenic in the crust. The same argument holds true for the upper mantle which is likely to be depleted by another factor of 10 below the lower crust concentrations. We therefore believe that the source of the anomaly is tectonic rather than radiogenic, and that the probable source of the anomaly is a zone of elevated temperatures at depth resulting from an intrusion from the asthenosphere, or some thermal process within the asthenosphere.

## Thermal Models and their Geodynamic Implications

Two interpretive models involving temperature perturbations at depth are considered in order to explain the broad observed heat-flow anomaly. In the plate tectonics framework the first model corresponds to the lithosphere coming to rest over one or several asthenospheric hotspots or convective upwellings. Burke and Wilson (1972) suggest that such an event happened to the African plate 25 Myr ago. In support of their hypothesis they cite such geologic evidence as the termination of the Walvis ridge just east of magnetic anomaly six, the lack of Neogene volcanic traces within the African plate, the changed pattern of Indian Ocean spreading, and the marked increase in volcanic activity, all occurring about 25 Myr ago. Evidence for a mid-Tertiary standstill may also be found in an analysis of Upper Tertiary paleomagnetic results from

the African plate (Piper and Richardson, 1972), which likewise demonstrate no detectable movement of the plate relative to the geographic pole for about the last 25 Myr. Briden and Gass (1974) have recently added further support for such a standstill model of the African plate with their recognition of a significant correlation between the timing of major African igneous and metamorphic episodes and pauses in the motion in the African plate as determined from the apparent polar wander path.

This first model involves the computation of surface heat flow in time following a sudden increase in temperature at the base of a slab. The transient response of the surface gradient is given (after Carslaw and Jaeger, 1959, p. 99) by

$$\frac{\partial T}{\partial z}\Big|_{z=0} = \frac{\Delta T}{\ell}\left[1 + 2\sum_{n=1}^{\infty}(-1)^n \exp\left(-n^2\pi^2\frac{\alpha t}{\ell^2}\right)\right]$$

where $\ell$ is the slab thickness, $\Delta T$ is the temperature step at $z = \ell$, $\alpha$ is thermal diffusivity, and $t$ is time elapsed since the temperature step occurred. This solution is shown in Figure 9 for $\Delta T = 100$ K and $\alpha = 32$ km$^2$/Myr; the time $t$ (Myr) identifies individual curves. The equilibrium surface gradient perturbation ($t = \infty$) is inversely proportional to the slab thickness, and as the slab thickness increases a progressively longer time is required before the full effect is seen at the surface.

To explain the Zambian anomaly of 15 mW m$^{-2}$, assuming a mean thermal conductivity of 3 W m$^{-1}$ K$^{-1}$, I seek conditions capable of producing a surface gradient perturbation of 5 K km$^{-1}$. Although the set of conditions is not unique, I can find a limiting depth below which the temperature perturbation required to produce the observed surface anomaly

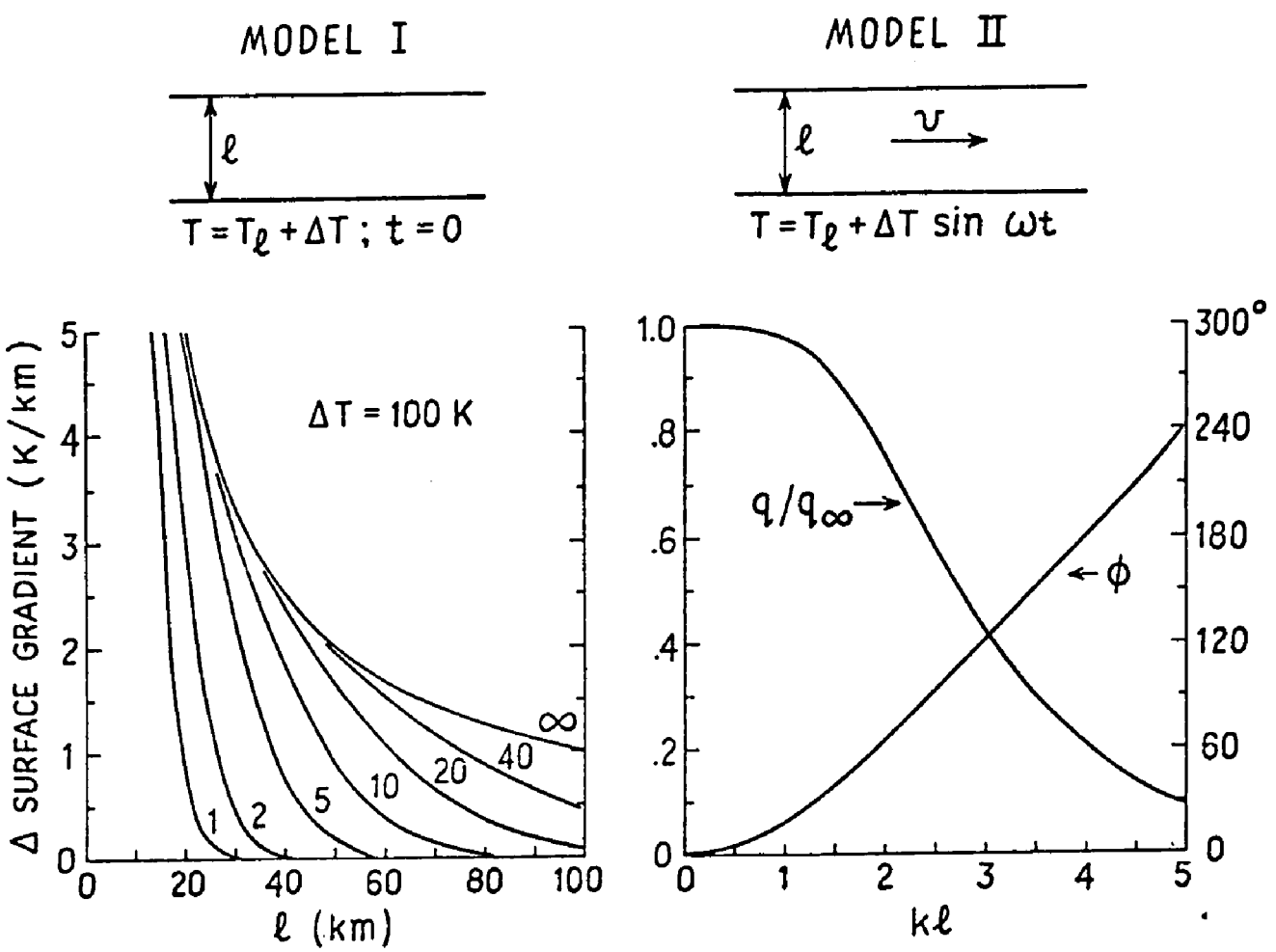



Figure 9. Thermal models showing response at the surface to specified temperature perturbations at depth. Model I: step temperature perturbation at base of slab ℓ km thick; curves are labeled by time (Myr) since the start of perturbation, and give change in surface gradient. Model II: time periodic perturbation at base of slab ℓ km thick; curves give attenuation $q/q_\infty$ and phase shift $\phi$ of the surface heat flow as functions of a dimensionless parameter $K\ell$ (defined in text).

becomes unacceptably large. For example, if 300 K represents a reasonable upper limit to the size of the temperature step then the steady surface gradient perturbation of 1.67 K $km^{-1}$/100 K step (i.e., 5 K $km^{-1}$/ 300 K step) in Figure 9 limits the source to depths less than 60 km. Correspondingly shallower depths to the temperature perturbation are obtained if it is still in a transient state: e.g., the depth must be 50 km for a step 20 Myr ago, and 33 km for a step 5 Myr ago.

A second model involves a temperature perturbation which is spatially periodic at the base of a moving slab (Pollack and Chapman, 1974). This corresponds to the lithosphere moving over a regular spatially periodic array of hotspots and coldspots in the asthenosphere, which, for a given element of lithosphere acts as an oscillatory (time periodic) lower boundary condition. This results in an upward-propagating thermal wave which is both attenuated and phase shifted at the surface. The temperature perturbation T is given (after Carslaw and Jaeger, 1959, p. 105) by

$$T = A(z) \sin [\omega t - \phi(z)]$$

where

$$\begin{matrix} A(z) \\ \phi(z) \end{matrix} = \begin{matrix} \text{mod} \\ \arg \end{matrix} \left[ \frac{\sinh Kz \quad (1+i)}{\sinh K\ell \quad (1+i)} \right]$$

and

$$K = \left( \frac{\omega}{2\alpha} \right)^{1/2} = \left( \frac{\pi}{\alpha \tau} \right)^{1/2}$$

The thermal wave number K depends on the thermal diffusivity $\alpha$ and the period $\tau$, which may be considered as the time required for an element of lithosphere to pass from hotspot to hotspot. The perturbed temperature gradient at the surface due to the periodic disturbance at depth is not

conveniently expressed, but is easily computed. Figure 9 shows the ratio of surface flux q to the equilibrium flux $q_\infty$ of an infinitely long period wave (i.e.: a steady perturbation) and the surface phase shift as functions of the dimensionless parameter $K\ell$. The value of $K\ell$ depends explicitly on the slab thickness $\ell$ and the period of the disturbance, which in turn is dependent on the spacing between hot spots and the velocity of the plate. The values of $K\ell$ that are obtained for a hotspot spacing of 1000 km and for a range of slab thicknesses and relative velocities are given in Table 5. Values of $K\ell$ for a hotspot spacing of 2000 km would be reduced by a factor $\sqrt{2}$

TABLE 5

Values of the Dimensionless Parameter $K\ell$ for Geophysically Relevant Combinations of Plate Thicknesses and Plate Velocities, and Perturbation Wavelength of 1000 km

| | plate velocity relative to source | | |
|---|---|---|---|
| plate thickness | fast (10 cm/yr) | slow (1 cm/yr) | very slow (0.1 cm/yr) |
| 50 km | 5 | 1.6 | 0.5 |
| 100 km | 10 | 3.2 | 1.0 |
| 150 km | 15 | 4.8 | 1.5 |

Allowing for uncertainty in the spatial characteristics of the source array, it appears that the geophysically interesting values of $K\ell$ lie between 0 and perhaps 20. It is apparent from Figure 9, however, that observable heat-flow anomalies will be associated only with parameters less than about 3, as many thermal disturbances at the base of the lithosphere are unlikely to be detected as heat flow perturbations at the surface, due to the attenuation of the upward propagating thermal wave.

With respect to the Zambian anomaly, the effect of this attenuation would be to place a restriction on the depth to the spatially periodic perturbation and on the velocity at which the plate moves across it. The parameter $K\ell$ can be no greater than 1 if the disturbance is at 60 km depth, and the observed surface heat flow anomaly is to be accounted for. For $\ell$ = 60 km, the wave number constrains the basal perturbation to a period greater than 350 Myr, or equivalently to a plate velocity less than .03 cm $yr^{-1}$ over a hotspot array with characteristic spacing of 1000 km. If $K\ell$ is assumed to have a value greater than about 2, corresponding to plate motions of a few centimeters a year relative to the source array, then the increased attenuation of the thermal wave requires considerably shallower source depths to obtain the necessary surface heat flow anomaly. For still greater value of $K\ell$ no appreciable heat flow anomaly will appear at the surface. Whichever of the two examined models is applicable, the corresponding source of the thermal anomaly cannot lie deeper than about 60 km, and if the source is an intrusion from, or the upper boundary of, the asthenosphere, it represents a considerable penetration into, or thinning of a Precambrian age continental lithosphere.

## Contemporary Tectonics of the African Rift System

High heat flow in Zambia resulting from a lithospheric thinning and/or penetration is consistent with other indications mentioned briefly in the introduction that the central African plateau south of Lake Tanganyika is in a dynamic state and responding to contemporary stress. In Figure 1 geophysical data have been compiled which place the Central African plateau in context with the entire African rift system south of the equator.

The seismic activity of the system is represented by the epicenters of earthquakes of magnitude 3.0 or greater for the period 1965 to 1970 as listed in the International Seismological Centre (Edinburgh) Regional Catalogue of Earthquakes. Notwithstanding the general diffuse nature of the seismicity the epicenters fall into recognizable zones with aseismic regions representing the more stable areas of the Kaapvaal, Rhodesia, Tanzania and Congo cratons. One distinct seismic belt follows the topographic Western Rift and leads southward into Mozambique. A second zone of earthquake activity extends south and west of the above mentioned belt in three roughly parallel southwest-trending bands: along the Upemba trough in southeastern Zaire; from Lake Tanganyika through Lake Mweru with a pronounced concentration in western Zambia; and along the Luangwa valley, through the Middle Zambezi valley and into northern Botswana.

Earthquake-source mechanisms are available for eight large earthquakes in the area shown in Figure 1, including four from western and southern Zambia (Maasha and Molnar, 1972, Table 1). These mechanisms imply a predominantly WNW-ESE tensional pattern accompanied by normal faulting. A recent microearthquake study by Scholz, et al. (1976) in Botswana has provided two additional composite source mechanisms from microearthquakes in northeastern Botswana which are consistent with mechanisms further to the north. This study also determined that microearthquake activity as far south as Lake Ngami is presently at a level comparable to that in the East African section of the rift. It appears therefore that the rift system seismicity extends to about $23^{o}$S and is approximately constant in level and source mechanism throughout.

Two studies are available on the propagation of seismic waves

throughout the rift system. Gumper and Pomeroy (1970) found East Africa to be characterized by low $P_n$ velocities and high $S_n$ attenuation particularly evident in, but not restricted to, rift zones north of the equator. Examination of their results (Gumper and Pomeroy, 1970, Figure 10) reveals no direct correlation between regions of poor $S_n$ propagation and the geographical extent of the surficial rift features. Also, Zambia seems to be a mixed region with some paths showing good $S_n$ propagation and others poor. A similar pattern of seismic velocities was obtained by Fairhead and Girdler (1971) using travel-time delays for paths with epicentral distance less than $30^{\circ}$. They mapped regions of low $P_n$ and found especially pronounced low velocities in the Gregory Rift north of $5^{\circ}$ S, but found no anomalous propagation in the region between the Eastern and Western rifts, nor to the south of the volcanic zones in Kenya.

A recent magnetometer array study (de Beer, et al., 1975) has revealed an electrical conductivity anomaly at crustal depths crossing from South West Africa into Botswana and western Rhodesia. The extent of this anomalous conductor is also shown in Figure 1. From west to east the conductive zone has an east-west arm running through South West Africa which broadens south of the Okavango delta and turns northward, approximately in line with the northeast-southwest Luangwa-middle Zambezi rift lineament. However, this northeast-trending conductivity anomaly is broader by a factor of two to three than these old surficial rift features and is in equally good alignment with several of the anomalous heat-flow sites. The origin of a conductivity anomaly may be either thermal or compositional or both, the former being associated with anomalously high temperatures in the crust and upper mantle, and

the latter with conductive materials which are commonly concentrated in fracture zones. The actual determination of origin thus depends on auxiliary geophysical and geological evidence. For example, conductivity anomalies under the Kenya Rift (Banks and Ottey, 1974) are interpreted as zones of partial melting in the upper mantle because they coincide with the low velocity and low density zones indicated by seismic and gravity investigations and are closely related spatially to regions of late Quaternary volcanic activity. De Beer, et al. (1975) prefer a fracture zone for the Botswana anomaly, but our new heat-flow data suggest that the origin may be at least partly thermal. A magnetometer array study across Zambia could provide the necessary complementary data to determine whether the Botswana conductivity anomaly is confined to the Zambezi-Luangwa trend or whether it broadens to the northwest across the heat flow anomaly.

Not shown on Figure 1 but important to a discussion of rifting, are the results of gravity investigations. The recently completed reconnaissance gravity survey of Zambia (I. M. Cowan and H. N. Pollack, personal communication, 1975) forms an important link between the extensive work in East Africa (see Wohlenberg, 1975, for summary) and the national surveys of Malawi (Andrew, 1974) and Botswana (Reeves and Hutchins, 1975). Although interpretation of the Zambian data is still in progress, some salient observations can be made. Significant differences are observed between Bouguer anomaly vs. elevation regressions in rift (Luangwa, Zambezi) and non-rift settings. These regression differences are similar in nature to those described for Kenya by Khan and Mansfield (1971) who have used the differences to infer abnormal crustal structure within the Gregory Rift. Two other features pertinent

to hypotheses of current rifting are the existence of a strong gravity low in a topographically flat region to the south of the western Zambia epicenter cluster, though it may indicate a buried Karroo age trough; the distinct gravimetric break corresponding to the known surface geologic interruption between the lower Luangwa and middle Zambezi valley, indicates an en echelon configuration similar to the Rukwa and Tanganyika rifts, rather than a continuity of structure.

## Comparison of Rift Tectonics

The global system of rift valleys, including both the mid-ocean ridges and their continental counterparts comprises one of the most prominent features on the earth. Within this rift system a genetic sequence may be inferred leading from an initial continental or oceanic rift through a young ocean (Red Sea stage) and finally to a mature and widening ocean (Atlantic stage) (Heezen, 1969). Modern rift zones should therefore provide information about the processes at work in the early stages of plate breakup.

A comparison of geological and geophysical characteristics of four modern intra-plate rift zones is shown in Table 6. Common to all zones is a history of Tertiary volcanism followed by uplift and finally graben formation. Predominantly normal faults are observed over a zone some 30 to 70 km wide, with the inferred lateral extension being approximately 5 km. All four rifts occur in plateaus having an elevation between 1000 and 2000 m. The thermal state of the four zones is likewise very similar. Surface heat flow is plotted in Figure 10 as a function of distance from the rift axis, and shows quite clearly a common high heat-flow peak with amplitude above flank levels of 30 to 60 mW $m^{-2}$ and an

TABLE 6

Geological and Geophysical Comparison of Modern Rifts

| Characteristic | Kenya rift | Rhinegraben | Baikal rift | Rio Grande rift |
|---|---|---|---|---|
| Volcanism | Miocene to present | Early Tertiary through Miocene | Paleocene to Plio-Pleistocene | throughout Tertiary |
| Uplift | slight (300 m) in Late Miocene; major uplift (1400 m) Late Pliocene to mid-Pleistocene | uplift simultaneous with trough subsidence since Mid Eocene; maximum structural elevation 2500 m | Pliocene-Pleistocene uplift; amplitude 3000 - 4000 m | |
| Rifting | | | | |
| (a) timing | first extensive faults in Early Pliocene | mid Eocene | Pliocene-Pleistocene | Late Miocene |
| (b) faulting | normal faults; throws of 3000-4000 m | normal faults | asymmetric normal faults; throws up to 5000 m | normal faults |
| (c) width of rift zone | 60 - 70 km | typically 36 km | about 30 km | |
| Subcrustal structure | Broad zone of low density, low seismic velocity ($v_p$ = 6.5 km/s) mantle below rift | Broad cushion of low seismic velocity ($v_p$ = 7.6 - 7.7 km/s) at depth 24 km below rift | Hot upper mantle at depth of 80 km below rift inferred from magnetotellurics and gravity | Low density, hot upper mantle inferred from gravity |
| Sources | Morgan, 1973 | Illies, 1972 | Florensov, 1969; Lubimova, 1969 | Decker and Smithson, 1975 |

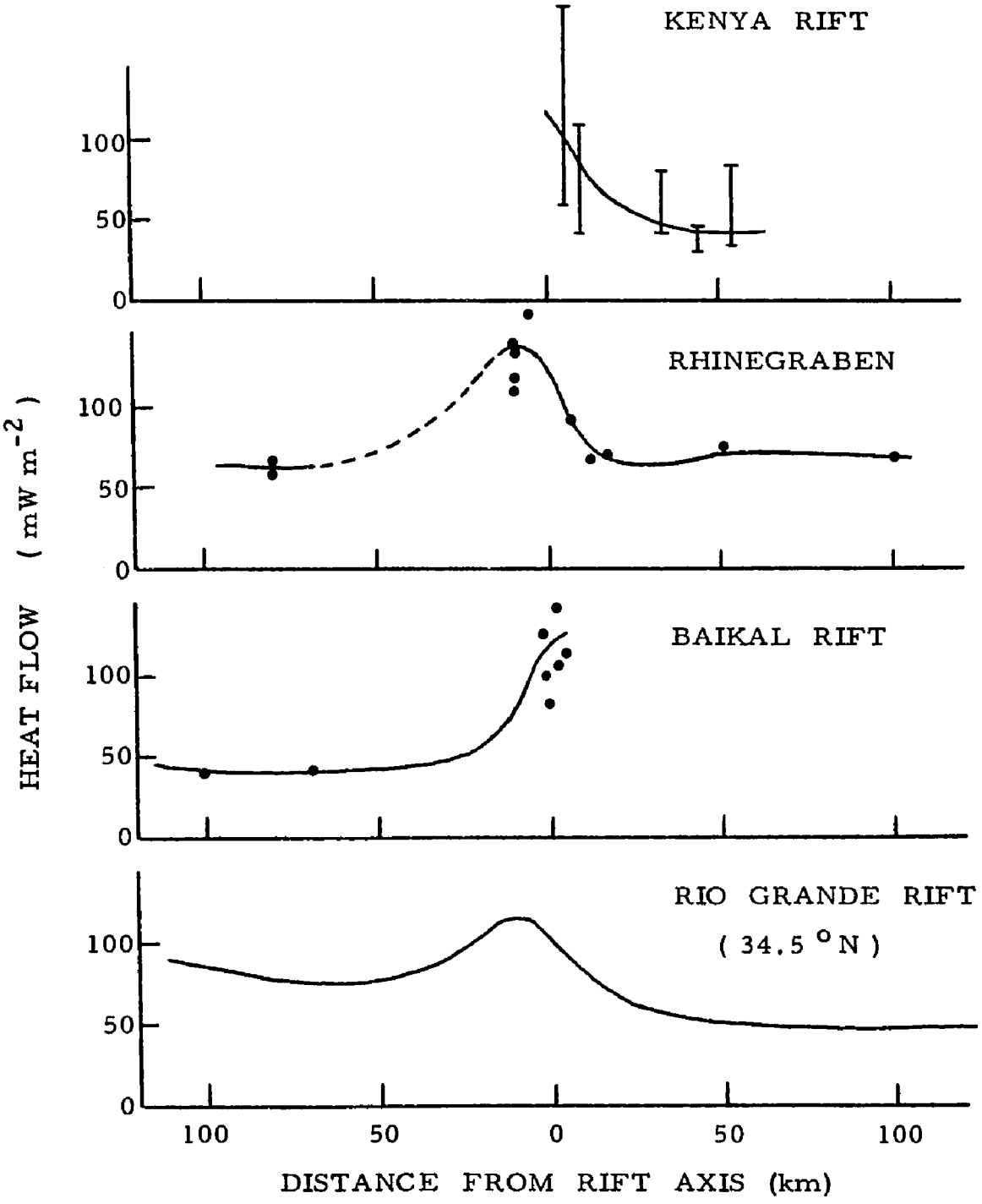



Figure 10. Heat flow from four modern continental rift zones plotted as a function of distance from the rift axis. Vertical bars indicate measurement uncertainties or scatter within groups of individual measurements. Sources: Kenya rift, Morgan, 1973; Rhinegraben, Haenel, 1970; Baikal rift, Lubimova, 1969; Rio Grande rift, Reiter, et al., 1975.

anomaly half width of about 20 km. The sharp boundary to the anomaly is most plausibly explained by transient effects of recent crustal magmatic penetration (Lubimova, 1969; Morgan, 1973; Decker and Smithson, 1975).

At upper mantle depths below the rifts there exists a much broader cushion of low density, low seismic velocity material which may be partially molten. In East Africa, evidence for this broad thermal zone is found not only from gravity, seismological and electrical conductivity studies (Sowerbuts, 1969; Gumper and Pomeroy, 1970; Banks, 1974) but more directly from the distribution of volcanics well outside the rift and removed from the fault scarps. The timing of initial volcanism provides a minimum age for the development or emplacement of this hot mantle cushion, 25 Myr in Kenya, but closer to 60 Myr in the other zones (Table 6). From Figure 9 it is evident that a thermal perturbation at a depth of several tens of kilometers (i.e., the proposed depth to the hot mantle cushion) will develop a significant fraction of its ultimate surface heat-flow perturbation after 25 Myr and nearly all of its ultimate surface perturbation after 60 Myr. Thus the absence of enhanced heat flow on the flanks of the Kenya and Baikal rifts and the Rhinegraben resulting from the hot mantle cushion remains a puzzle and warrants further attention. A broad region of high heat flow is observed on the western flank of the Rio Grande rift and extends into the Basin and Range physiographic province.

The magnitude, breadth, and flatness of the western Zambia thermal anomaly are consistent with a region underlain by anomalously hot mantle, not unlike the deep thermal structure proposed for the East African, Baikal, Rhine and Rio Grande rifts. It is clear from the absence of Tertiary volcanics and Recent graben formation that western Zambia has

not proceeded to the active rifting stage. However, the observed thermal anomaly taken together with the active seismicity of the region, the extensional tectonics indicated by earthquake fault plane solutions, and the elevation of the plateau suggests that western Zambia may be in an incipient rift stage, thereby delineating a future southward extension of the East African rift system.

This preliminary hypothesis of incipient rifting in western Zambia is presently based on scant evidence and should be tested by some or all of the following studies: (1) extension of heat flow measurements to all geographic regions of Zambia to define the extent of the thermal anomaly; (2) magnetic variometer studies within Zambia and Rhodesia to map the northward continuation of the Botswana electrical conductivity anomaly (de Beer, et al., 1965; also see Figure 1); (3) microearthquake studies concentrated in western Zambia to map active faults and to determine composite fault-plane solutions across the thermal anomaly; (4) seismic refraction experiments utilizing Copperbelt mine blasts to determine the local seismic velocity structure; and (5) seismometer array studies of teleseismic travel time variations to investigate mantle velocity structure below western Zambia.

# CHAPTER IV

## CONCLUSIONS

Several hypotheses have been advanced concerning the southern termination of the East African rift system. A popular plate construction (Dietz and Holden, 1970) pictures the African Rift running through Lake Malawi and the Shire Rift to the Mozambique channel, thereby delineating the southwest boundary of the Somalia subplate. An alternative suggestion is that an arm of the active rift extends southwestward from Lake Tanganyika across the central African plateau (Fairhead and Girdler, 1969). A variant of this alternative suggestion is that the Luangwa-Middle Zambezi lineament marks a propagating rift extension through eastern and southern Zambia into Botswana (Scholz, et al., 1976). Yet another alternative (Girdler, 1975) is that the long wavelength negative Bouguer gravity anomaly that is so prominent on the African gravity map of Sletene, et al. (1973) may indicate the presence of an incipient rift west-southwest of Lake Tanganyika. Over East Africa this negative gravity anomaly coincides with surface rift features and has been interpreted as indicating regions of thinned lithosphere.

There is a varying amount of support for each of the suggested trends. The southern trend through Malawi and Mozambique is supported by strong seismicity and Quaternary surface rift features. The southwest trend through Zambia and into Botswana is supported by the alignment of the Botswana electrical conductivity anomaly, long wavelength

residual gravity trends in Zambia, and by seismicity of the area, much of which is unrelated to present fault zones. The western trend is supported only by the topography and its associated large negative Bouguer gravity anomaly.

My discovery of a broad heat-flow anomaly and the inference of thinned lithosphere in west and central Zambia, provides additional support for the southwest rift-extension hypothesis. The extent of the thermal anomaly is presently unbounded in all directions except to the southeast where current work (E. R. Oxburgh, personal communication, 1975) indicates normal to sub-normal heat flow on the Rhodesian craton. An important objective for future heat flow and other geophysical measurements in Central Africa will be to prove the extend of the anomalous thermal zone and to discriminate between the rift extension hypotheses.

## APPENDIX I

## CONSTRUCTION AND CALIBRATION OF HEAT-FLOW EQUIPMENT

### Temperature Probes

The main features and dimensions of the temperature probes are shown in Figure 11. The body of the probes was machined from 3/4 inch brass stock, and includes a cavity for electrical connections and a cylindrical gasket for clamping and sealing the probe to the borehole cable. Interchangeable thermistor housings are fitted to the front of the probe with a standard pipe thread and O-ring seal.

The temperature transducer itself is a thermistor assembly mounted in the end of a narrow stainless steel tube, filled with lubricant to facilitate thermal contact with the tube wall. Characteristics of the commercial assemblies used in this study are given below.

| Characteristic | Thermistor assembly | |
|---|---|---|
| | Fenwal K212E | YSI 403 |
| probe length | 146 mm | 114 mm |
| probe diameter | 4.2 mm | 4.0 mm |
| thermistor beads | 20 | 1 |
| nominal resistance (25 C) | 10,000 Ω | 3,000 Ω |
| sensitivity at 25 C | 0.002 K/Ω | 0.010 K/Ω |
| power dissipation in still water | 55 mW/K | 5 mW/K |
| time constant | 5 s | 4 s |

### Thermistor Calibration and Stability

All thermistor probes were calibrated by measuring their resistances in a temperature controlled bath, the temperature of which was determined

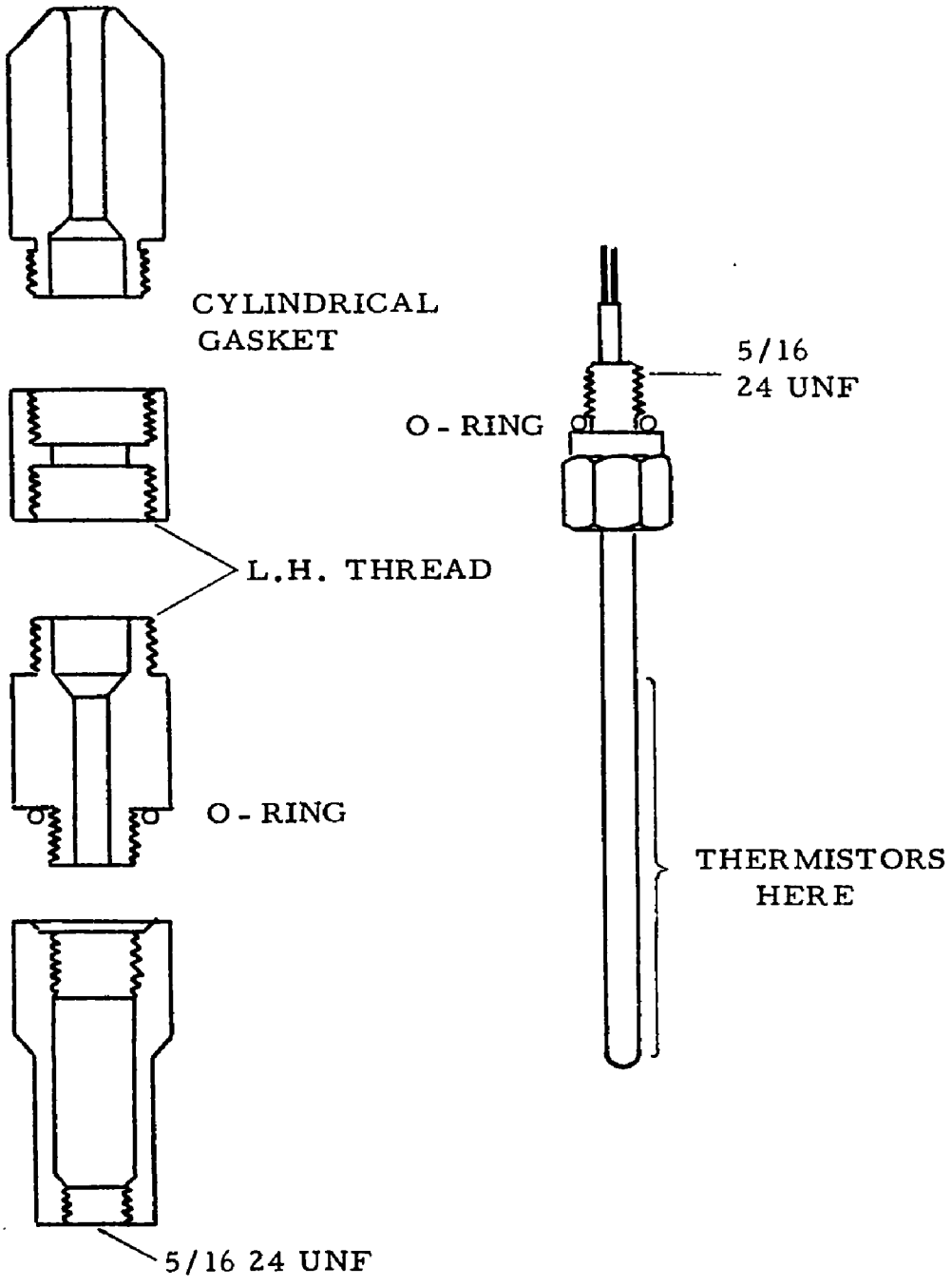



Figure 11. Thermistor probe assembly. Thermistor(s) are sealed in thin wall stainless steel tube (right) which is attached to brass housing (left) facilitating electrical connection and clamping to borehole cable.

with a Hewlet Packard 2801A quartz thermometer having a 0.001 K resolution. Calibration accuracy for the quartz thermometer is claimed to be ± 0.02 K absolute, traceable to the National Bureau of Standards. For each probe, seven resistance-temperature pairs were obtained at approximately 10 K intervals between $0^{o}C$ and $60^{o}C$. When magnetic stirring of the bath was employed the temperature could be controlled to within ± 0.01 K for a period of several minutes. On the first calibration, a magnetic stirrer was not available, and instead a drift technique was employed whereby four cycles of temperature and resistance were measured in regular order, and the temperature-resistance calibration values were interpolated. Measurement uncertainities resulting from the equipment used and techniques employed are estimated to be ± 1 ohm and ± 0.01 K in resistance and temperature values respectively.

Subsets of three resistance-temperature points were used to determine the calibration constants A, B, and C of the equation

$$R = \exp(A + \frac{B}{T + C})$$

where R is the thermistor resistance at temperature $T^{o}C$. Temperature residuals were then calculated for all remaining calibration points. If one or two of the seven possible calibration points could be identified as causing relatively large residuals, they would be eliminated. Generally at least five calibration points remained for which a single curve of the above form could be fitted for the temperature range $0^{o}C$ to $50^{o}C$, and for which the residuals nowhere exceed 0.05 K. Best fitting sets of calibration constants for three probes are given in Table 7(a) for two calibrations conducted in April, 1973 and June, 1975. The 1973 constants were used to compute a calibration table of temperatures corresponding

TABLE 7(a)

Thermister Calibration Constants and Drift Characteristics

| Calibration | | Thermistor calibration constants | | |
|---|---|---|---|---|
| Date | Probe | A | B(°C) | C(°C) |
| April, 1973 | M 1 | -4.3887 | 4870.4 | 330.88 |
| | M 2 | -3.8959 | 4531.3 | 318.51 |
| | M 3 | -4.9020 | 5234.3 | 343.79 |
| June, 1975 | M 1 | -3.9123 | 4524.7 | 317.63 |
| | M 2 | -3.7407 | 4546.0 | 318.55 |
| | M 3 | -3.4339 | 4209.2 | 305.73 |

to 1 ohm increments of resistance over the desired temperature range for each probe. These tables are the basis for all temperatures reported in this study.

Possible errors introduced by thermistor instability may be assessed by comparing the two calibrations, separated in time by two years, of the Fenwal thermistor probes M 1, M 2, and M 3. During this period, probe M 3 had been used for more than 50 temperature surveys, whereas M 1 and M 2 had not been used in the field. The calibration constants are shown in Table 7(a) and the temperatures computed from those constants for fixed resistances are given in Table 7(b). The apparent thermistor drift in Table 7(b) will include both real drift and also calibration uncertainties. Several more calibrations will be required before these effects can be separated. The apparent drift in two years is 0.1 K or less for most of the working temperature range.

Of greater consequence in heat flow calculations is the differential temperature drift $\frac{\partial}{\partial T}(T_{drift})$, which affects the temperature gradient calculation. This quantity is given in Table 7(c), and is less than 0.5% over the temperature range of interest. I therefore conclude, as

TABLE 7(b)

Details of Thermistor Drift, ΔT

| Resistance (Ω) | Probe M 1 | | | Probe M 2 | | | Probe M 3 | | |
|---|---|---|---|---|---|---|---|---|---|
| | T 1975 | T 1973 | ΔT | T 1975 | T 1973 | ΔT | T 1975 | T 1973 | ΔT |
| 6,000 | 41.14 | 41.24 | -.10 | 41.10 | 41.25 | -.15 | 41.18 | 41.02 | +.16 |
| 8,000 | 33.14 | 33.24 | -.10 | 33.09 | 33.21 | -.12 | 33.14 | 33.05 | +.09 |
| 10,000 | 27.17 | 27.26 | -.09 | 27.13 | 27.23 | -.10 | 27.16 | 27.09 | +.07 |
| 12,000 | 22.45 | 22.52 | -.07 | 22.40 | 22.48 | -.08 | 22.43 | 22.36 | +.07 |
| 14,000 | 18.55 | 18.62 | -.07 | 18.50 | 18.57 | -.07 | 18.54 | 18.45 | +.09 |

TABLE 7(C)

Differential Thermistor Drift

| Ambient temp | $\frac{\partial}{\partial T}(T_{drift})$ Probe M 1 | Probe M 2 | Probe M 3 |
|---|---|---|---|
| 21°C | -.2% | -.4% | -.3% |
| 26°C | +.1% | -.4% | -.3% |
| 32°C | +.4% | -.4% | -.2% |

have others (see Roy, et al., 1968a, Table 1) that thermistor instability is a negligible source of error for heat flow determinations.

## Cables and Reel

Three lightweight borehole cables (Northern Electric, 4 conductor, 26 solid PEI, fiberglass filler, PVC jacket) of lengths 600 m, 600 m, and 1200 m were prepared and used in this study. The 600 m cables were marked at 10 m intervals and the 1200 m cable at 20 m intervals by cementing length coded heat shrinkable tubing onto epoxy smears. Odd multiples of 10 m were marked with a 10 mm length of tubing, even multiples of 10 m with a 20 mm length of tubing, and multiples of 100 m with

additional 5 mm lengths of tubing. The length calibration was checked periodically, but the permanent strain after two years use was found to be negligible.

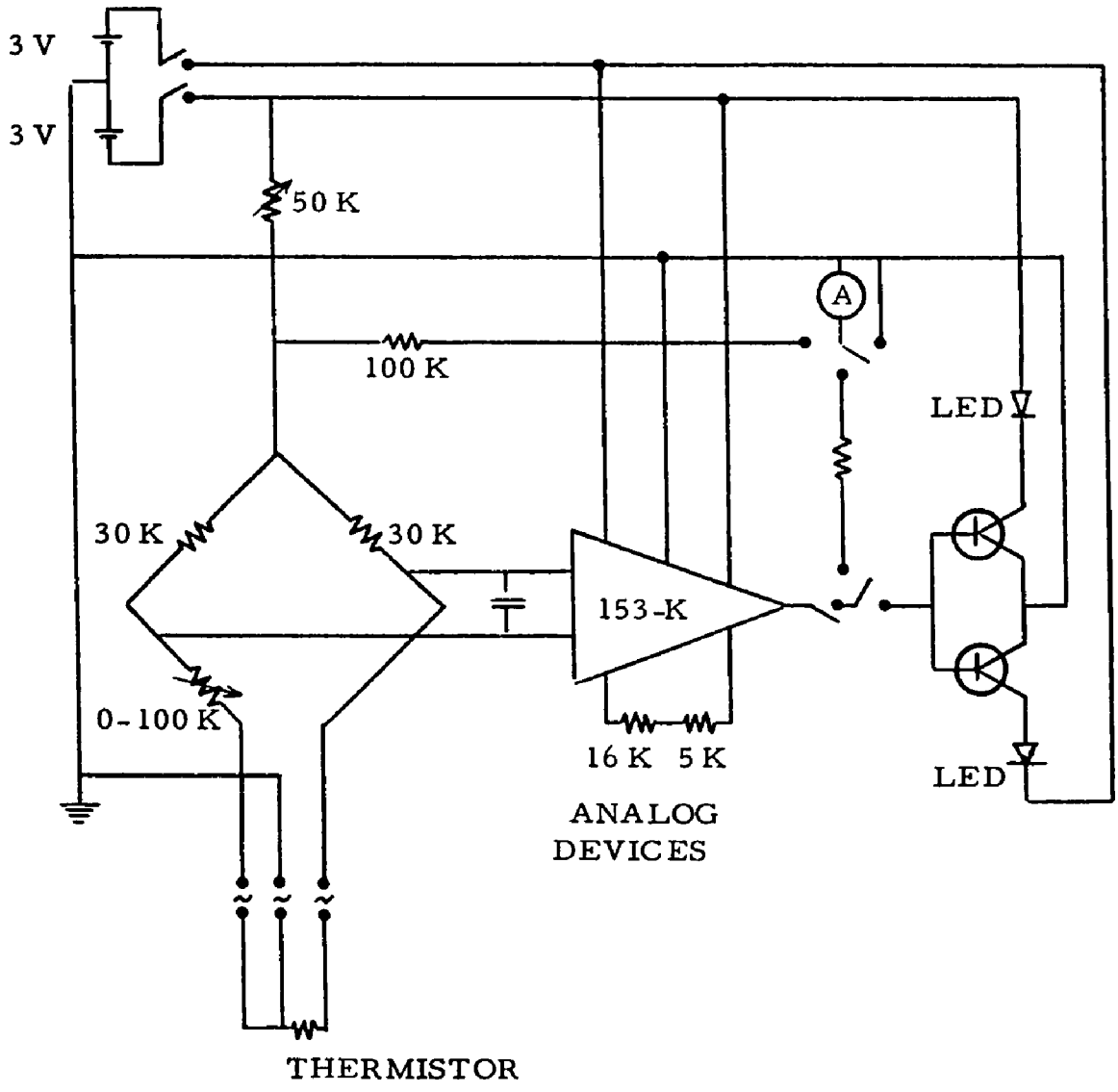
Portable geophysical reels type GR 400 obtained from Edgar Sharpe Ltd., capable of holding about 1500 m of this borehole cable, were ideally suited for the purpose. Portability was stressed in the design of all components of the system. The probe, reel with 600 m of cable, and electrical bridge together with packing crates weigh only 30 kg.

## Resistance Bridge

Two resistance bridges were used during this study. Prior to 1973, temperatures were measured with a commercially available Doran E3379 portable Wheatstone bridge modified for a three conductor connection. The 1973 and all subsequent measurements, which included resurveys of some of the earlier drillholes, were made with a higher sensitivity and more robust resistance bridge assembled from components. The circuit diagram for this second bridge is shown in Figure 12. The null detector part of the circuit was designed to operate in a binary mode, with switch-over occurring when the bridge was balanced. This balance condition could be observed either on a Weston taut band microammeter, or alternatively on a pair of shockproof light emitting diodes.

## Divided Bar Construction

The geometry and dimensions of the divided bar apparatus are shown in Figure 13. Interchangeable stacks have been constructed with diameters of 33, 42, 54.6 and 72.5 mm., corresponding to the most common sizes of drill core encountered. An Enerpac RC 50 hydraulic pump is used to maintain 100 psi line pressure for all measurements. The entire bar is




BRIDGE RESISTORS
FIXED: ESI RCR 30 K; TC MATCH 0.5 PPM/°C
VARIABLE: ESI DS 1464 0-12 K
ESI 12 U 0-100 K (10 K STEP)

Figure 12. Circuit diagram for resistance bridge.

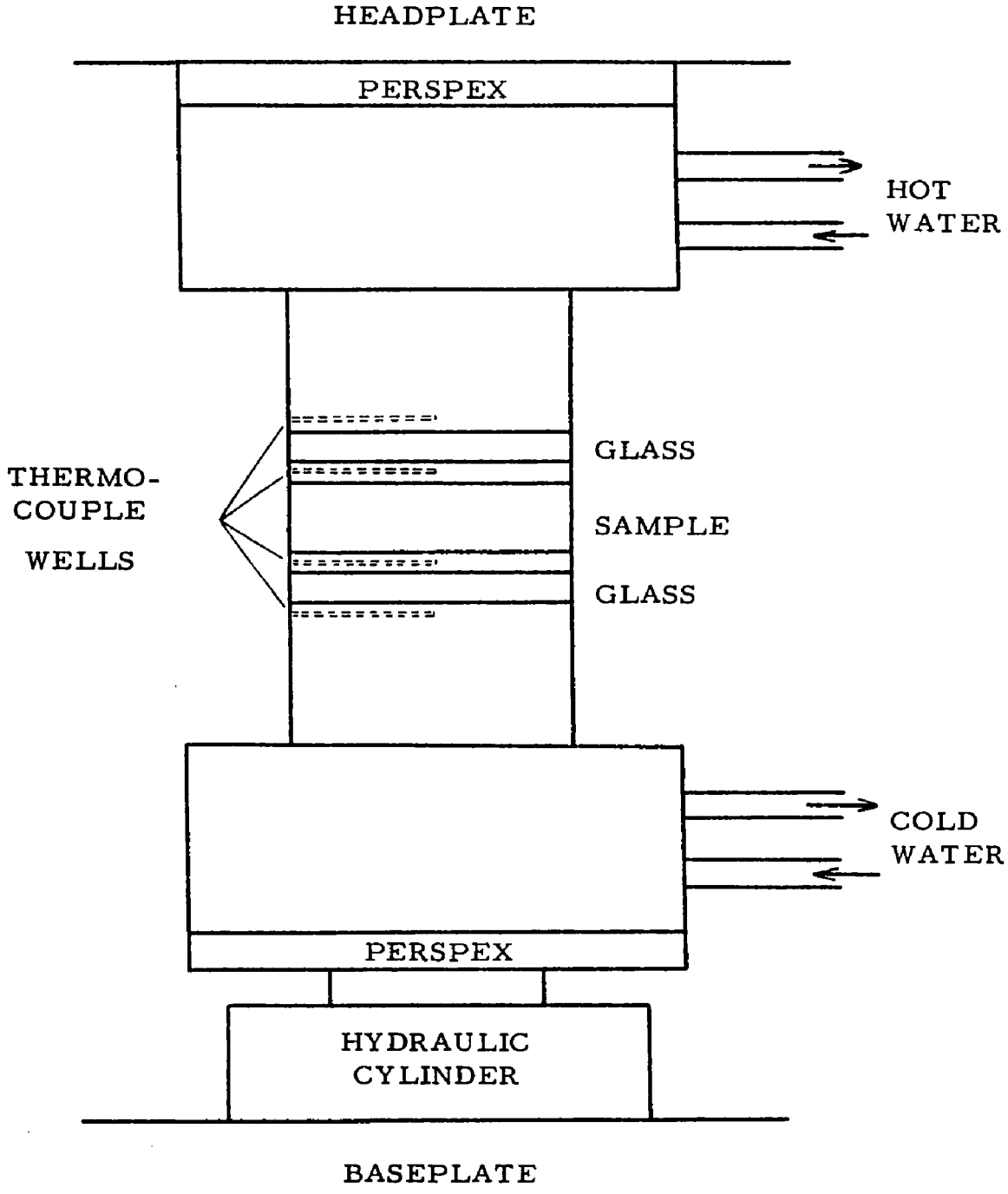



Figure 13. Schematic diagram of the divided-bar thermal conductivity apparatus.

thermally insulated with a minimum of 5 cm. thick close fitting styrofoam.

Two Haake Type FE variable power temperature controllers are used to maintain constant temperatures at the ends of the stack. The temperature transducers are Omega Engineering Inc. chromel-constantin thermocouples with a thermal emf of 63 $\mu V\ K^{-1}$, connected in differential mode to Precision Digital Type STC-7 thermocouple switch. All temperature readings are made with a Doric DS 100 digital microvoltmeter, and since the data reduction involves temperature ratios only, the working temperature unit is thermocouple microvolts.

The thermal conductivity reference discs were Amersil commercial grade CFQ discs 1/8 inch thick, ground and polished flat and parallel to 0.025 mm tolerance. These discs were permanently cemented into the stack using Delta Bond 152-2, a high thermal conductivity epoxy.

The calibration standards were fused silica type GE 101 discs supplied by E.B.L. Company Inc. For the absolute value of the thermal conductivity of fused silica, Ratcliffe's (1959) results

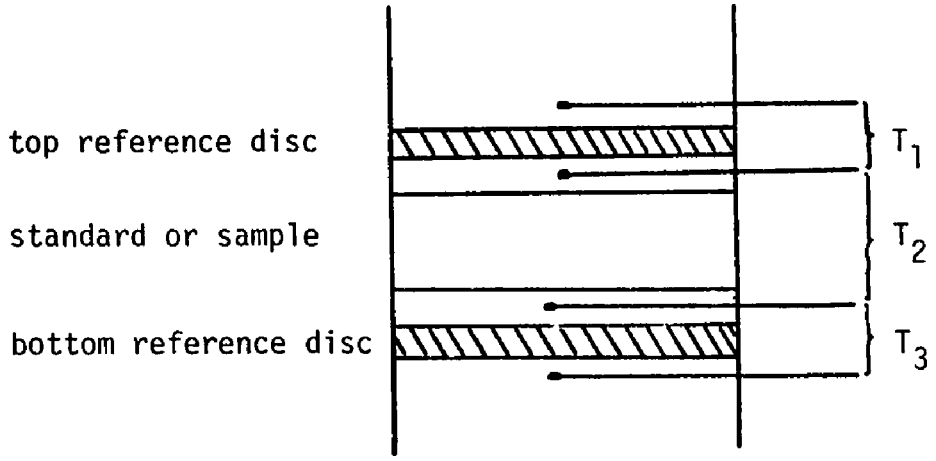
$$k_{\text{fused silica}} = 4.186 \times 10^{-4}[3160. + 4.6T - 0.016T^2]\ Wm^{-1}K^{-1}$$

has been adopted in accordance with practice in other geothermal laboratories (Roy, et al., 1968; Sass, et al., 1971; Jessop, 1968; Beck, 1965).

## Calibration of the Divided Bar

Consider the divided bar shown schematically below with extreme ends held at constant and different temperatures, such that $T_1$, $T_2$, and $T_3$ are the respective steady state temperature drops across the top reference disc, the quartz standard or rock sample, and the bottom

reference disc as shown.




In subsequent discussion only $T_1$ will be used for the reference disc temperature drop although in all calculations the mean of $T_1$ and $T_3$ is employed. The calibration constants for a given divided bar are defined from the following way considerations.

Assuming no radial heat loss between temperature transducers across the reference disc, the temperature drop $T_1$ will be given by

$$T_1 = \left(\frac{z}{k}\right)_{ref} q_1 \qquad (1)$$

where z is the effective thickness and k the effective thermal conductivity of the composite reference disc including epoxy bonds contacts and sandwiched copper, and $q_1$ is the axial heat flow through the disc. Similarly the temperature drop $T_2$ will be given by

$$T_2 = \left[\left(\frac{z}{k}\right)_{Q \text{ or } S} + R_2\right] q_2 \qquad (2)$$

where it is now necessary to separate the thickness z and conductivity k of the quartz standard "Q" or sample "S" from the total contact

resistance $R_2$. Let

$$q_2 = q_1 + \varepsilon \tag{3}$$

where $\varepsilon$ is some constant heat loss in the stack. A more general relationship would be

$$q_2 = \lambda q_1 + \varepsilon;\ \lambda \leq 1 \tag{4}$$

but as $\lambda$ cannot be determined by the calibration procedure, (3) is used. From equations 1, 2, and 3, we obtain

$$T_2 = T_1 \frac{1}{(z/k)_{ref}} \{(\frac{z}{k})_Q + R_2\} + \varepsilon\{(\frac{z}{k})_Q + R_2\} \tag{5}$$

Now define S and I as the slope and intercept of $T_1$ vs. $T_2$ curves, obtained for several thicknesses of the quartz standard.

$$S = \frac{\partial T_2}{\partial T_1} = \frac{1}{(z/k)_{ref}} \{(\frac{z}{k})_Q + R_2\}$$

and

$$I = T_2|_{T_1=0} = \varepsilon \{(\frac{z}{k})_Q + R_2\} .$$

Then

$$\frac{\partial S}{\partial (z/k)_Q} = \frac{1}{(z/k)_{ref}} = A\ ;\quad S|_{z_Q=0} = \frac{R_2}{(z/k)_{ref}} = B$$

$$\frac{\partial I}{\partial (z/k)_Q} = \varepsilon = C \qquad ;\quad I|_{z_{Q=0}} = \varepsilon R_2 = D$$

identify the calibration constants A, B, C, and D.

If a sample S is now substituted for the quartz standard Q, and letting primes denote the new parameters,

$$T_2' = T_1' \frac{1}{(z/k)_{ref}} \{(\frac{z}{k})_s + R_2'\} + \varepsilon' \{(\frac{z}{k})_s + R_2'\}$$

Solving for $k_s$

$$k_s = \frac{z_s [T_1' \frac{1}{(z/k)_{ref}} + \varepsilon']}{T_2' - [T_1' \frac{R_2}{(z/k)_{ref}} + \varepsilon' R_2']}$$

and assuming $R_2' = R_2$, and $\varepsilon' = \varepsilon$ then

$$k_s = z_s \frac{[AT_1' + C]}{T_2' - (BT_1' + D)}$$

In practice, the temperature baths were set, and $T_1$ and $T_2$ pairs recorded for each of four fused quartz discs of thickness 2.5, 5.0, 7.5 and 10.0 mm. This procedure was repeated several times for total temperature drops varying between 0 and 16 K with the mean temperature held fixed so that the quartz standard conductivity remained constant in all cases. The resulting data were fit successively by least squares methods to yield the calibration constants.

The constants for the four divided bars calibrated at a mean temperature of 26°C and an adopted thermal conductivity of fused quartz at 26°C of 1.368 W $m^{-1}$ $K^{-1}$ are given in Table 8.

The values for C and for B/A permit evaluation of the heat loss $\varepsilon$ and the contact resistance $R_2$ respectively. Typically, $\varepsilon$ is 0.5% of $q_1$ and $R_2$ is about 3% of the thermal resistance of an average sample. Thus

TABLE 8

Divided Bar Calibration Constants

| Bar Diameter (mm) | A $\frac{(Wm^{-1}K^{-1})}{mm}$ | B | C $\frac{\mu V(Wm^{-1}K^{-1})}{mm}$ | D $\mu V$ |
|---|---|---|---|---|
| 33 | 0.386 | 0.042 | 0.392 | -0.907 |
| 42 | 0.389 | 0.033 | -0.152 | -0.542 |
| 54.6 | 0.378 | 0.026 | 0.248 | -0.784 |
| 72.5 | 0.376 | 0.032 | 0.712 | -1.945 |

the assumptions made that $\varepsilon' = \varepsilon$ and $R_2' = R_2$ are unlikely to lead to significant errors.

## Corrections for Undersized and Oversized Discs

The correction factors to be used for diameter mismatch in a divided bar are given by Jaeger and Beck (1965). If the diameter of the disc '2d' is less than the divided bar diameter '2a', the measured apparent conductivity $k_a$ will be low, and the true conductivity k is given by

$$k = k_a \left(\frac{2a}{2d}\right)^2$$

On the other hand, if the diameter of the disc is greater than the bar diameter, then the apparent conductivity of the sample will be high because of refraction of the lines of flow into the outer ring of the sample, and the true conductivity is given

$$k = k_a \left\{1 - \frac{16}{\pi^2} \Sigma \frac{I_1(\frac{n\pi a}{\ell})}{n^2 I_1(\frac{n\pi d}{\ell})} \cdot \left[I_1\left(\frac{n\pi d}{\ell}\right) K_1\left(\frac{n\pi a}{\ell}\right) - K_1\left(\frac{n\pi d}{\ell}\right) I_1\left(\frac{n\pi a}{\ell}\right)\right]\right\}$$

where $I_1$ and $K_1$ are the modified Bessel functions of the order unity,

$\ell$ is the disc thickness, a the bar radius, d is the disc radius, and the summation is performed over the odd values n = 1, 3, 5, ... . For computation purposes the following polynomial approximations for $I_1(x)$ and $K_1(x)$ were used (Abramowitz and Stegun, 1966, p. 378).

$$I_1(x) = [0.39894 - 0.03988\ t^{-1} - 0.00362\ t^{-2}]\ e^x\ x^{-1/2}$$

$$\text{where } t = \frac{x}{3.75}$$

$$K_1(x) = [1.25331 + 0.23409(\tfrac{2}{x}) - 0.03655(\tfrac{2}{x})^2]\ x^{-1/2}\ e^{-x}$$

The undersized disc correction has been tested by measuring discs on two larger diameter bars and comparing the corrected conductivities. Such a comparison is shown in Table 9 for three samples.

TABLE 9

Comparison of Disc Thermal Conductivity Values Corrected for Diameter Mismatch

| Sample | Diameter | 33 mm bar | | | 42 mm bar | | | % diff. in corr. values |
|---|---|---|---|---|---|---|---|---|
| | mm | $k_a$ $(\frac{W}{mK})$ | $k_{corr.}$ $(\frac{W}{mK})$ | corr. (%) | $k_a$ $(\frac{W}{mK})$ | $k_{corr.}$ $(\frac{W}{mK})$ | corr. (%) | (%) |
| COL 5 750 | 31.95 | 3.17 | 3.38 | 7 | 1.99 | 3.44 | 73 | 2 |
| DS 4 95 | 30.00 | 2.31 | 2.80 | 21 | 1.47 | 2.88 | 96 | 3 |
| DS 4 106 | 29.97 | 1.40 | 1.70 | 21 | 0.88 | 1.74 | 98 | 2 |

In all cases excellent agreement has resulted: for actual corrections to the apparent conductivity of up to 100% the corrected conductivities differ by less than 3%.

The oversize disc correction has been tested in a similar way on

rock samples and quartz standards, but without similar success. For corrections to the apparent conductivity of less than 50% the corrected conductivities differ consistently by 5 to 10%. Therefore, whenever a diameter mismatch has occurred, it has been standard procedure to measure the sample on an oversized bar and to apply the more reliable undersize disc correction.

# APPENDIX II

## HEAT FLOW DATA FROM ZAMBIA

Early papers on terrestrial heat flow included detailed discussions of methods and techniques and were abundantly documented by tables of basic data. The recent practice in reporting heat flow results has been to accumulate data from several sites in a region and to publish all values at once with a considerably abbreviated discussion of techniques and a virtual absence of detailed documentation. This appendix contains tabulations of basic heat flow data, thereby making available to critical readers the relevant details for each borehole utilized in this study. The data includes: site location, geographic coordinates, and elevation; drilling and measurement dates; borehole inclination; temperature-depth values; thermal conductivity-depth values; and a summary geologic log. The following parameters used in computing heat flow are also given: depth-range (depth interval over which the heat flow calculation is performed); conductivity (harmonic mean thermal conductivity of the samples within the depth range) in units of $W\ m^{-1}K^{-1}$; gradient (least squares straight line gradient fitted to the temperature depth data in the given depth range in units of $mK\ m^{-1}$; heat flow (calculated as the product of conductivity and gradient values in units of $mW\ m^{-2}$. Uncertainties given for conductivity, gradient and heat flow are the respective standard errors of the means.

Province: Northwestern
Locality: Malundwe
Borehole: MMB 152

Site latitude: 12° 14' S
Site longitude: 25° 49' E
Site elevation: 1290 ± 10 m
Completed by: 1962
Surveyed on: March 31, 1971
Dip angle: 90°

Depth range 120-209 M
N: 19
Conductivity: 2.65 ± 0.11
Gradient: 21.4 ± 0.4
Heat flow: 57 ± 8

| depth (m) | T (°C) |
|---|---|
| 20.3 | 20.49 |
| 40.6 | 21.03 |
| 60.9 | 21.75 |
| 71.2 | 22.14 |
| 81.4 | 22.45 |
| 91.7 | 22.75 |
| 102.1 | 22.99 |
| 112.6 | 23.23 |
| 123.1 | 23.54 |
| 133.6 | 23.76 |
| 144.4 | 24.01 |
| 155.1 | 24.22 |
| 165.8 | 24.46 |
| 176.5 | 24.67 |
| 187.3 | 24.91 |
| 198.0 | 25.15 |
| 208.6 | 25.35 |

| depth (m) | k (W/mK) |
|---|---|
| 23 | 3.62 |
| 31 | 2.42 |
| 38 | 2.32 |
| 47 | 2.13 |
| 58 | 2.64 |
| 66 | 3.37 |
| 75 | 3.49 |
| 85 | 3.46 |
| 99 | 2.70 |
| 103 | 2.33 |
| 109 | 2.61 |
| 125 | 2.11 |
| 151 | 2.87 |
| 172 | 2.75 |
| 180 | 3.03 |
| 188 | 3.66 |
| 195 | 2.52 |
| 208 | 2.17 |
| 215 | 2.70 |

| to depth (m) | geology |
|---|---|
| 99 | granite gneiss |
| 202 | quartz mica schist with feldspar, kyanite and garnet |
| 210 | kyanite, epidote quartz mica schists |

Province: Northwestern
Locality: Malundwe
Borehole: MMB 553

Site latitude: 12° 14' S
Site longitude: 25° 49' E
Site elevation: 1290 ± 10 m
Completed by: July 21, 1970
Surveyed on: April 1, 1971
Dip angle: 90°

Depth range: 40-113 m
N: 11
Conductivity: 2.76 ± 0.18
Gradient: 24.9 ± 1.7
Heat flow: 69 ± 6

| depth (m) | T (°C) |
|---|---|
| 20 | 22.72 |
| 41 | 22.99 |
| 51 | 23.22 |
| 61 | 23.46 |
| 71 | 23.64 |
| 81 | 23.96 |
| 92 | 24.24 |
| 102 | 24.53 |
| 113 | 24.81 |

| depth (m) | k (W/mK) |
|---|---|
| 31 | 2.09 |
| 36 | 2.93 |
| 45 | 3.33 |
| 51 | 3.39 |
| 58 | 2.09 |
| 67 | 3.36 |
| 74 | 3.58 |
| 80 | 1.94 |
| 89 | 2.51 |
| 105 | 3.20 |
| 111 | 2.61 |

| to depth (m) | geology |
|---|---|
| 16 | weathered schist |
| 27 | quartz mica schist |
| 29 | quartzite |
| 80 | quartz-feldspathic gneiss |
| 127 | quartz mica schist |

Province: Northwestern
Locality: Chimiwungo
Borehole: MM 632

Site latitude: 12° 17' S
Site longitude: 25° 53' E
Site elevation: 1340 ± 10
Completed by: October 22, 1971
Surveyed on: June 12, 1973
Dip angle: 84°

Depth range: 20-163 m
N: 13
Conductivity: 2.43 ± 0.14
Gradient: 22.1 ± 0.37
Heat flow: 54 ± 6

| depth (m) | T (°C) |
|---|---|
| 20 | 22.24 |
| 30 | 22.48 |
| 40 | 22.70 |
| 50 | 22.90 |
| 60 | 23.10 |
| 70 | 23.34 |
| 80 | 23.58 |
| 90 | 23.79 |
| 100 | 24.00 |
| 110 | 24.24 |
| 120 | 24.45 |
| 130 | 24.67 |
| 140 | 24.90 |
| 150 | 25.12 |
| 160 | 25.34 |
| 163 | 25.42 |

| depth (m) | k (W/mK) |
|---|---|
| 30 | 2.24 |
| 50 | 3.19 |
| 50 | 3.16 |
| 60 | 2.47 |
| 70 | 1.51 |
| 90 | 3.06 |
| 100 | 2.70 |
| 110 | 2.21 |
| 120 | 3.04 |
| 130 | 1.92 |
| 140 | 2.80 |
| 150 | 2.35 |
| 160 | 2.31 |

| to depth (m) | geology |
|---|---|
| 22 | weathered feldspathic schist |
| 31 | muscovite schist |
| 56 | feldspathic gneiss |
| 62 | muscovite schist |
| 91 | feldspathic schist/gneiss |
| 142 | muscovite schist, feldspathic bands, minor amphibolite |
| 185 | quartz biotite feldspar gneiss |

Province: Northwestern
Locality: Chimiwungo
Borehole: MM 655

Site latitude: 12° 17' S
Site longitude: 25° 53' E
Site elevation: 1340 ± 10 m
Completed by: November 19, 1971
Surveyed on: June 9, 1973
Dip angle: 81°

Depth range: 60-140 m
N: 9
Conductivity: 2.16 ± 0.23
Gradient: 24.0 ± 0.83
Heat Flow: 52 ± 6

| depth (m) | T (°C) |
|---|---|
| 10 | 21.61 |
| 20 | 22.11 |
| 30 | 22.61 |
| 40 | 22.78 |
| 50 | 22.96 |
| 60 | 23.05 |
| 70 | 23.14 |
| 80 | 23.28 |
| 90 | 23.55 |
| 100 | 23.80 |
| 110 | 24.01 |
| 120 | 24.25 |
| 130 | 24.50 |
| 140 | 24.75 |

| depth (m) | k (W/mK) |
|---|---|
| 50 | 2.48 |
| 60 | 2.69 |
| 70 | 2.06 |
| 80 | 2.62 |
| 90 | 2.67 |
| 100 | 2.63 |
| 110 | 2.90 |
| 130 | 1.51 |
| 140 | 1.59 |

| to depth (m) | geology |
|---|---|
| 15 | weathered gneiss |
| 46 | feldspathic gneiss |
| 51 | muscovite schist |
| 85 | interbanded schist, gneiss and amphibolite |
| 118 | muscovite schist with bands of feldspathic schist and amphibolite |
| 147 | interbanded quartz biotite feldspar schist, gneiss and amphibolite |

Province: Northwestern
Locality: Chimiwungo
Borehole: MMC 458

Site latitude: 12° 17' S
Site longitude: 25° 53' E
Site elevation: 1340 ± 10 m
Completed by: August 15, 1969
Surveyed on: April 2, 1971
Dip angle: 90°

Depth range: 20-175 m
N: 19
Conductivity: 2.17 ± 0.12
Gradient: 20.5 ± 1.5
Heat flow: 45 ± 4

| depth (m) | T ( C) |
|---|---|
| 20 | 22.18 |
| 41 | 22.57 |
| 61 | 23.05 |
| 81 | 23.40 |
| 102 | 23.97 |
| 113 | 24.23 |
| 123 | 24.34 |
| 134 | 24.56 |
| 144 | 24.74 |
| 155 | 24.92 |
| 166 | 25.11 |
| 175 | 25.35 |

| depth (m) | k (W/mK) |
|---|---|
| 40 | 2.65 |
| 48 | 2.26 |
| 55 | 2.95 |
| 63 | 2.40 |
| 69 | 2.22 |
| 94 | 2.25 |
| 105 | 2.83 |
| 109 | 1.60 |
| 113 | 2.39 |
| 118 | 2.17 |
| 121 | 2.48 |
| 124 | 3.60 |
| 128 | 1.97 |
| 131 | 1.52 |
| 138 | 2.84 |
| 148 | 2.62 |
| 156 | 2.27 |
| 165 | 1.13 |
| 171 | 1.91 |

| to depth (m) | geology |
|---|---|
| 18 | weathered schist |
| 136 | quartz mica schists with garnet, feldspar, kyanite |
| 183 | generally porphyroblastic quartz mica schist |

Province: Northwestern
Locality: Chimiwungo
Borehole: MMC 705

Site latitude: 12° 17' S
Site longitude: 25° 53' E
Site elevation: 1340 ± 10
Completed by: May 29, 1973
Surveyed on: June 9, 1973
Dip angle: 90°

Depth range: 20-140 m
N: 12
Conductivity: 2.70 ± 0.24
Gradient: 24.7 ± 1.03
Heat flow: 67 ± 7

| depth (m) | T (°C) | depth (m) | k (W/mK) |
|---|---|---|---|
| 20 | 21.96 | 50 | 3.48 |
| 30 | 22.24 | 60 | 3.31 |
| 40 | 22.55 | 70 | 4.46 |
| 50 | 22.77 | 80 | 2.03 |
| 60 | 22.95 | 90 | 2.72 |
| 80 | 23.45 | 100 | 2.06 |
| 90 | 23.71 | 110 | 1.93 |
| 100 | 23.98 | 120 | 3.70 |
| 110 | 24.22 | 130 | 1.72 |
| 120 | 24.48 | 140 | 4.13 |
| 130 | 24.72 | 150 | 2.58 |
| 140 | 24.95 | 160 | 3.53 |

| to depth (m) | geology |
|---|---|
| 32 | weathered schist |
| 52 | schist |
| 128 | muscovite schist |
| 136 | quartz-biotite-feldspar schist |
| 152 | interbraided porphyroblastic schist and quartz mica schist |

Province: Northwestern
Locality: Lubwe
Borehole: MMD 468

Site latitude: 12° 10' S
Site longitude: 25° 57' E
Site elevation: 1356 ± 10 m
Completed by: September 13, 1969
Surveyed on: April 3, 1971
Dip angle: 90°

Depth range: 20-176 m
N: 18
Conductivity: 2.21 ± 0.11
Gradient: 24.5 ± 2.5
Heat flow: 54 ± 6

| depth (m) | T (°C) |
|---|---|
| 20.3 | 21.66 |
| 30.4 | 21.82 |
| 40.6 | 21.97 |
| 50.8 | 22.13 |
| 60.9 | 22.35 |
| 71.2 | 22.69 |
| 81.4 | 23.17 |
| 91.7 | 23.47 |
| 102.1 | 23.76 |
| 112.6 | 23.99 |
| 123.1 | 24.20 |
| 133.6 | 24.40 |
| 144.4 | 24.58 |
| 155.1 | 24.73 |
| 165.8 | 24.93 |
| 176.5 | 25.08 |

| depth (m) | k (W/mK) |
|---|---|
| 22 | 3.26 |
| 27 | 2.95 |
| 47 | 2.25 |
| 54 | 2.66 |
| 64 | 2.03 |
| 72 | 2.37 |
| 78 | 2.36 |
| 87 | 2.74 |
| 95 | 1.82 |
| 102 | 1.49 |
| 109 | 1.48 |
| 118 | 2.15 |
| 132 | 1.91 |
| 142 | 2.25 |
| 146 | 2.75 |
| 155 | 2.96 |
| 162 | 2.39 |
| 168 | 1.97 |

| to depth (m) | geology |
|---|---|
| 16 | weathered schist |
| 186 | quartz mica schist with feldspar, garnet, kyanite and chlorite |

Province: Copperbelt
Locality: Ichimpe
Borehole: PE 2

Site latitude: 12° 44' S
Site longitude: 28° 07' E
Site elevation: 1210 ± 15 m
Completed by: June 1, 1973
Surveyed on: June 6, 1973
Dip angle: 85°

Depth range: 20-500 m
N: 11
Conductivity: 3.89 ± 0.20
Gradient: 19.0 ± 0.83
Heat flow: 74 ± 5

| depth (m) | T (°C) |
|---|---|
| 20.0 | 22.46 |
| 40.0 | 22.71 |
| 60.0 | 23.05 |
| 80.0 | 23.57 |
| 100.0 | 23.87 |
| 120.0 | 24.29 |
| 140.0 | 24.50 |
| 160.0 | 24.82 |
| 180.0 | 25.19 |
| 200.0 | 25.55 |
| 220.0 | 25.90 |
| 240.0 | 26.23 |
| 260.0 | 26.57 |
| 280.0 | 26.99 |
| 300.0 | 27.38 |
| 320.0 | 27.78 |
| 340.0 | 28.19 |
| 360.0 | 28.59 |
| 380.0 | 29.03 |
| 400.0 | 29.54 |
| 420.0 | 30.09 |
| 440.0 | 30.46 |
| 460.0 | 30.74 |
| 480.0 | 31.16 |
| 500.0 | 31.63 |

| depth (m) | k (W/mK) |
|---|---|
| 79 | 4.38 |
| 160 | 3.41 |
| 180 | 3.73 |
| 200 | 3.88 |
| 220 | 5.60 |
| 240 | 3.11 |
| 260 | 4.03 |
| 281 | 3.80 |
| 319 | 4.01 |
| 359 | 3.34 |
| 379 | 4.54 |

| to depth (m) | geology |
|---|---|
| 50 | decomposed siliceous sandy dolomite |
| 92 | breccia conglomerate and siliceous dolomite |
| 117 | siliceous and albitized dolomite |
| 318 | breccia conglomerate with siliceous dolomite bands |
| 560 | siliceous dolomite with argillaceous bands |

Province: Copperbelt
Locality: Lumpuma
Borehole: Lup 7

Site latitude: 13° 05' S
Site longitude: 28° 03' E
Site elevation: 1204 ± 30 m
Completed by: August 4, 1973
Surveyed on: August 14, 1973
Dip angle: 90°

Depth range: 20-198 m
N: 19
Conductivity: 2.73 ± 0.14
Gradient: 23.6 ± 1.0
Heat flow: 65 ± 4

| depth (m) | T (°C) | depth (m) | k (W/mK) |
|---|---|---|---|
| 20.0 | 22.99 | 48 | 2.61 |
| 30.0 | 23.24 | 55 | 3.04 |
| 40.0 | 23.44 | 67 | 2.18 |
| 50.0 | 23.77 | 73 | 2.67 |
| 60.0 | 23.99 | 84 | 2.52 |
| 70.0 | 24.23 | 91 | 3.00 |
| 80.0 | 24.45 | 110 | 4.52 |
| 90.0 | 24.67 | 123 | 2.74 |
| 100.0 | 24.85 | 132 | 1.70 |
| 110.0 | 25.03 | 140 | 2.14 |
| 120.0 | 25.23 | 149 | 2.15 |
| 130.0 | 25.50 | 158 | 2.19 |
| 140.0 | 25.74 | 159 | 2.88 |
| 150.0 | 26.02 | 167 | 3.12 |
| 160.0 | 26.36 | 175 | 3.24 |
| 170.0 | 26.58 | 181 | 2.85 |
| 180.0 | 26.82 | 188 | 3.11 |
| 190.0 | 27.08 | 192 | 3.07 |
| 197.5 | 27.25 | | |

| to depth (m) | geology |
|---|---|
| 46 | meta siltstone |
| 56 | meta gabbro |
| 70 | meta siltstone |
| 158 | meta quartzite |
| 213 | amphibolite |

Comments:
Borehole resurveyed November 26, 1974 by J. Vise, University of Zambia. Results identical to above.

Province: Central
Locality: Mkushi
Borehole: COL 2

Site latitude: 13° 55' S
Site longitude: 29° 12' E
Site elevation: 1125 ± 15 m
Completed by: April 10, 1970
Surveyed on: July 19, 1971
Dip angle: 68°

Depth range: 114-279 m
N: 20
Conductivity: 3.24 ± 0.07
Gradient: 18.8 ± 0.3
Heat flow: 61 ± 2

| depth (m) | T (°C) |
|---|---|
| 18.8 | 23.42 |
| 28.2 | 23.55 |
| 37.6 | 23.74 |
| 47.1 | 23.93 |
| 56.5 | 24.15 |
| 66.2 | 24.36 |
| 75.9 | 24.56 |
| 85.6 | 24.69 |
| 95.4 | 24.79 |
| 105.4 | 24.93 |
| 114.9 | 25.08 |
| 124.4 | 25.24 |
| 134.2 | 25.42 |
| 143.9 | 25.61 |
| 153.6 | 25.80 |
| 163.3 | 25.98 |
| 173.1 | 26.18 |
| 182.8 | 26.35 |
| 192.4 | 26.55 |
| 201.5 | 26.72 |
| 210.7 | 26.90 |
| 220.2 | 27.07 |
| 229.6 | 27.24 |
| 239.4 | 27.42 |
| 249.1 | 27.60 |
| 259.1 | 27.77 |
| 269.1 | 27.94 |
| 279.2 | 28.12 |

| depth (m) | k (W/mK) |
|---|---|
| 26 | 2.91 |
| 38 | 3.18 |
| 48 | 2.98 |
| 54 | 3.51 |
| 62 | 3.11 |
| 70 | 3.10 |
| 77 | 3.10 |
| 85 | 2.94 |
| 91 | 3.19 |
| 108 | 2.84 |
| 117 | 3.10 |
| 121 | 3.17 |
| 133 | 3.01 |
| 137 | 3.96 |
| 147 | 3.59 |
| 156 | 3.49 |
| 173 | 3.28 |
| 181 | 3.53 |
| 186 | 3.14 |
| 195 | 3.00 |
| 204 | 3.00 |
| 211 | 3.09 |
| 229 | 3.69 |
| 238 | 2.93 |
| 245 | 3.53 |
| 252 | 3.09 |
| 260 | 2.95 |
| 267 | 3.16 |
| 273 | 2.92 |
| 277 | 3.57 |

| to depth (m) | geology |
|---|---|
| 12 | weathered zone |
| 280 | grey flaser type gneiss with numerous pegmatite and aplite veins, often chloritic |

Province: Central
Locality: Mkushi
Borehole: COL 5

Site latitude: 13° 55' S
Site longitude: 29° 12' E
Site elevation: 1125 ± 15 m
Completed by: July 11, 1971
Surveyed on: July 20, 1971
Dip angle: 55

Depth range: 64-201 m
N: 16
Conductivity: 2.98 ± 0.08
Gradient: 20.5 ± 0.7
Heat flow: 61 ± 3

| depth (m) | T (°C) |
|---|---|
| 16.4 | 23.00 |
| 24.4 | 23.14 |
| 32.5 | 23.38 |
| 40.5 | 23.62 |
| 48.4 | 23.82 |
| 56.3 | 24.00 |
| 64.1 | 24.22 |
| 71.9 | 24.45 |
| 79.7 | 24.59 |
| 87.5 | 24.73 |
| 95.2 | 24.88 |
| 102.8 | 25.02 |
| 110.6 | 25.20 |
| 118.2 | 25.39 |
| 125.7 | 25.54 |
| 133.1 | 25.67 |
| 140.5 | 25.81 |
| 147.7 | 25.92 |
| 154.8 | 26.08 |
| 161.6 | 26.23 |
| 168.2 | 26.38 |
| 175.0 | 26.54 |
| 181.7 | 26.68 |
| 188.1 | 26.80 |
| 194.5 | 26.92 |
| 200.9 | 27.05 |

| depth (m) | k (W/mK) |
|---|---|
| 19 | 2.84 |
| 22 | 2.59 |
| 28 | 2.99 |
| 36 | 2.84 |
| 43 | 3.15 |
| 51 | 3.36 |
| 57 | 3.01 |
| 63 | 3.13 |
| 69 | 3.19 |
| 74 | 3.08 |
| 80 | 2.91 |
| 87 | 2.99 |
| 94 | 2.90 |
| 102 | 2.88 |
| 110 | 2.92 |
| 118 | 2.66 |
| 125 | 2.71 |
| 132 | 2.79 |
| 140 | 3.01 |
| 148 | 3.20 |
| 162 | 3.78 |
| 170 | 3.52 |
| 178 | 3.06 |
| 184 | 2.55 |

| to depth (m) | geology |
|---|---|
| 201 | grey flaser type gneiss with numerous pegmatite and aplite veins, often chloritic |

Comments:

Borehole surveyed on July 18, 19 and 20. Uniform cooling was observed such that predicted equilibrium gradient was not significantly different from July 20 values used above.

Province: Central
Locality: Chalalobuka
Borehole: CH 78-42

Site latitude: 15° 13' S
Site longitude: 28° 33' E
Site elevation: 1110 ± 10 m
Completed by: November 18, 1970
Surveyed on: December 10, 1970
Dip angle: 90°

Depth range: 50-161
N: 11
Conductivity: 2.90 ± 0.25
Gradient: 22.0 ± 1.4
Heat flow: 64 ± 7

| depth (m) | T (°C) |
|---|---|
| 20.3 | 23.76 |
| 40.6 | 24.46 |
| 50.8 | 24.35 |
| 60.9 | 24.51 |
| 71.2 | 24.75 |
| 81.4 | 24.90 |
| 91.7 | 25.22 |
| 101.1 | 25.45 |
| 112.6 | 25.66 |
| 123.1 | 25.90 |
| 133.6 | 26.14 |
| 144.4 | 26.35 |
| 155.1 | 26.60 |
| 160.5 | 26.71 |

| depth (m) | k (W/mK) |
|---|---|
| 12 | 2.60 |
| 18 | 3.27 |
| 24 | 2.37 |
| 30 | 5.97 |
| 37 | 2.90 |
| 55 | 2.21 |
| 72 | 2.32 |
| 88 | 2.92 |
| 110 | 3.32 |
| 126 | 4.63 |
| 148 | 3.07 |

| to depth (m) | geology |
|---|---|
| 14 | weathered zone |
| 160 | granite gneiss with frequent bands of biotite schist and amphibolite schist |

Province: Central
Locality: Chalalobuka
Borehole: CH 70-7

Site latitude: 15° 13' S
Site longitude: 28° 33' E
Site elevation: 1110 ± 10 m
Completed by: April 5, 1971
Surveyed on: May 2, 1971
Dip angle: 90°

Depth range: 30-144 m
N: 16
Conductivity: 3.12 ± 0.19
Gradient: 23.0 ± 1.8
Heat flow: 72 ± 7

| depth (m) | T (°C) |
|---|---|
| 20.3 | 23.84 |
| 30.4 | 23.98 |
| 40.6 | 24.20 |
| 50.8 | 24.44 |
| 60.9 | 24.68 |
| 71.2 | 24.93 |
| 81.4 | 25.16 |
| 91.7 | 25.45 |
| 101.8 | 25.82 |
| 112.6 | 26.01 |
| 123.1 | 26.22 |
| 133.6 | 26.40 |
| 144.4 | 26.57 |

| depth (m) | k (W/mK) |
|---|---|
| 38 | 8.08 |
| 44 | 4.71 |
| 59 | 2.38 |
| 65 | 2.59 |
| 67 | 3.20 |
| 73 | 3.29 |
| 80 | 3.40 |
| 86 | 2.24 |
| 94 | 3.00 |
| 101 | 3.05 |
| 109 | 3.73 |
| 115 | 3.07 |
| 124 | 3.21 |
| 130 | 2.70 |
| 138 | 5.38 |
| 144 | 3.10 |

| to depth (m) | geology |
|---|---|
| 9 | weathered zone |
| 150 | granite gneiss with bands of biotite schist and amphibolite schists, garnetiferous in places |

Province: Central
Locality: Chalalobuka
Borehole: CH 59-12

Site latitude: 15° 13' S
Site longitude: 28° 33' E
Site elevation: 1110 ± 10 m
Completed by: March 2, 1971
Surveyed on: March 21, 1971
Dip angle: 90°

Depth range: 20-164 m
N: 13
Conductivity: 3.11 ± 0.11
Gradient: 21.9 ± 1.1
Heat flow: 68 ± 4

| depth (m) | T (°C) |
|---|---|
| 20.3 | 24.18 |
| 30.4 | 24.35 |
| 40.6 | 24.56 |
| 50.8 | 24.71 |
| 60.9 | 24.90 |
| 71.2 | 25.10 |
| 81.4 | 25.30 |
| 91.7 | 25.55 |
| 101.8 | 25.78 |
| 112.6 | 26.01 |
| 123.1 | 26.30 |
| 133.6 | 26.59 |
| 144.4 | 26.89 |
| 155.1 | 27.09 |
| 163.6 | 27.25 |

| depth (m) | k (W/mK) |
|---|---|
| 64 | 2.76 |
| 72 | 3.56 |
| 78 | 3.09 |
| 84 | 3.22 |
| 90 | 3.23 |
| 105 | 3.27 |
| 108 | 2.93 |
| 118 | 3.17 |
| 136 | 2.82 |
| 126 | 3.73 |
| 132 | 2.27 |
| 151 | 3.53 |
| 163 | 3.54 |

| to depth (m) | geology |
|---|---|
| 8 | weathered zone |
| 165 | granite gneiss with bands of biotite schist and amphibolite schist, garnetiferous below 92 m |

Province: Central
Locality: Chalalobuka
Borehole: CH 59-8

Site latitude: 15° 13' S
Site longitude: 28° 33' E
Site elevation: 1110 ± 10 m
Completed by: February 4, 1970
Surveyed on: March 21, 1971
Dip angle: 90°

Depth range: 20-150 m
N: 7
Conductivity: 2.63 ± 0.20
Gradient: 23.3 ± 1.3
Heat flow: 61 ± 6

| depth (m) | T (°C) |
|---|---|
| 20.3 | 23.90 |
| 30.4 | 24.18 |
| 40.6 | 24.50 |
| 50.8 | 24.79 |
| 60.9 | 24.94 |
| 71.2 | 25.12 |
| 81.4 | 25.35 |
| 91.7 | 25.60 |
| 101.1 | 25.83 |
| 112.6 | 26.08 |
| 123.1 | 26.35 |
| 133.6 | 26.60 |
| 144.4 | 26.90 |
| 149.7 | 27.00 |

| depth (m) | k (W/mK) |
|---|---|
| 40 | 2.10 |
| 59 | 3.14 |
| 75 | 3.65 |
| 94 | 2.54 |
| 109 | 2.87 |
| 135 | 2.45 |
| 146 | 2.26 |

| to depth (m) | geology |
|---|---|
| 30 | weathered zone |
| 150 | granite gneiss with bands of biotite schist and amphibolite schist |

Province: Southern
Locality: Munali Hills
Borehole: MH 23

Site latitude: 15° 55' S
Site longitude: 28° 09' E
Site elevation 1097 ± 10 m
Completed by: January 8, 1972
Surveyed on: May 23, 1973
Dip angle: 65°

Depth range: 70-309 m
N: 7
Conductivity: 2.82 ± 0.11
Gradient 22.6 ± 0.6
Heat flow 64 ± 3

| depth (m) | T (°C) |
|---|---|
| 73.4 | 26.66 |
| 83.0 | 26.84 |
| 92.8 | 27.02 |
| 102.6 | 27.25 |
| 112.4 | 27.48 |
| 122.2 | 27.68 |
| 132.3 | 27.91 |
| 141.7 | 28.16 |
| 150.6 | 28.39 |
| 159.4 | 28.61 |
| 168.4 | 28.79 |
| 177.3 | 28.96 |
| 186.0 | 29.12 |
| 194.6 | 29.29 |
| 203.1 | 29.48 |
| 211.9 | 29.68 |
| 220.7 | 29.90 |
| 229.1 | 30.12 |
| 237.8 | 30.38 |
| 246.6 | 30.56 |
| 255.4 | 30.78 |
| 264.3 | 30.97 |
| 273.3 | 31.15 |
| 282.2 | 31.33 |
| 291.2 | 31.52 |
| 300.0 | 31.72 |
| 309.1 | 31.93 |

| depth (m) | k (W/mK) |
|---|---|
| 183 | 3.09 |
| 197 | 3.03 |
| 215 | 2.33 |
| 222 | 2.54 |
| 270 | 2.93 |
| 277 | 3.03 |
| 304 | 3.01 |

| to depth (m) | geology |
|---|---|
| 13 | weathered zone |
| 103 | quartzite with limestone bands |
| 120 | calcareous biotite schist |
| 140 | serpentinized gabbro |
| 173 | medium grain gabbro, partly brecciated |
| 282 | gabbro |
| 292 | gabbro, highly talcose |
| 310 | gabbro |

Comments:
Borehole surveyed on January 9 and February 26, 1972; May 18 and May 23, 1973. Final survey values used in heat flow calculation.

Province: Southern
Locality: Munali Hills
Borehole: MH 43

Site latitude: 15° 55' S
Site longitude: 28° 08' E
Site elevation: 1097 ± 10 m
Completed by: May 14, 1973
Surveyed on: May 31, 1973
Dip angle: 65°

Depth range: 27-290 m
N:
Conductivity: 2.82 ± 0.11*
Gradient: 22.6 ± 0.5
Heat flow: 64 ± 3

| depth (m) | T (°C) |
|---|---|
| 18.1 | 25.66 |
| 27.2 | 25.98 |
| 36.2 | 26.19 |
| 45.3 | 26.48 |
| 54.4 | 26.66 |
| 63.4 | 26.83 |
| 72.5 | 27.02 |
| 81.6 | 27.24 |
| 90.6 | 27.42 |
| 99.7 | 27.61 |
| 108.8 | 27.81 |
| 117.8 | 28.00 |
| 126.9 | 28.19 |
| 135.9 | 28.40 |
| 145.0 | 28.61 |
| 154.1 | 28.81 |
| 163.1 | 29.03 |
| 172.2 | 29.24 |
| 181.3 | 29.47 |
| 190.3 | 29.66 |
| 199.4 | 29.86 |
| 208.4 | 30.07 |
| 217.5 | 30.31 |
| 226.6 | 30.50 |
| 235.6 | 30.72 |

| depth (m) | k (W/mK) |
|---|---|
| (temperatures continued) | |
| 244.7 | 30.93 |
| 253.8 | 31.16 |
| 262.8 | 31.33 |
| 271.9 | 31.54 |
| 280.9 | 31.72 |
| 290.0 | 31.86 |

| to depth (m) | geology |
|---|---|
| | entire hole in gabbro |

Comments:
Borehole measured on May 22, 23 and 31, 1973. Gradient unchanged between May 23 and 31.

*Conductivity value taken from MH 23 gabbro samples average.

Province: Southern
Locality: Lubombo
Borehole: LUB 1

Site latitude: 15° 49' S
Site longitude: 27° 55' E
Site elevation: 1009 ± 3 m
Completed by: January 15, 1973
Surveyed on: May 21, 1973
Dip angle: 90°

Depth range: 40-360 m
N: 10
Conductivity: 2.81 ± 0.09
Gradient: 25.4 ± 0.40
Heat flow: 71 ± 3

| depth (m) | T (°C) |
|---|---|
| 10 | 26.57 |
| 20 | 26.09 |
| 40 | 26.27 |
| 50 | 26.47 |
| 60 | 26.69 |
| 70 | 26.91 |
| 80 | 27.15 |
| 90 | 27.36 |
| 100 | 27.59 |
| 110 | 27.82 |
| 120 | 28.06 |
| 130 | 28.30 |
| 140 | 28.56 |
| 150 | 28.84 |
| 160 | 29.11 |
| 170 | 29.40 |
| 180 | 29.65 |
| 190 | 29.96 |
| 200 | 30.22 |
| 210 | 30.47 |
| 220 | 30.74 |
| 230 | 30.98 |
| 240 | 31.21 |
| 250 | 31.47 |
| 260 | 31.71 |
| 270 | 31.96 |
| 280 | 32.21 |
| 290 | 32.46 |

| depth (m) | k (W/mK) |
|---|---|
| 47 | 2.35 |
| 59 | 3.07 |
| 79 | 3.07 |
| 91 | 2.43 |
| 106 | 3.00 |
| 121 | 2.90 |
| 136 | 2.90 |
| 197 | 3.20 |
| 183 | 2.60 |
| 229 | 2.88 |

(temperatures continued)

| | |
|---|---|
| 300 | 32.70 |
| 310 | 32.98 |
| 320 | 33.24 |
| 340 | 33.52 |
| 350 | 33.76 |
| 360 | 34.23 |

| to depth (m) | geology |
|---|---|
| 20 | weathered zone |
| 95 | garnetiferous biotite schist |
| 161 | feldspathic gneiss, partly conglomeratic |
| 201 | alternating gneiss, hornblendite and granite |
| 235 | coarse pink granite with amphibolite bands |
| 250 | amphibolite |
| 259 | pegmatite |
| 312 | gabbro, alternating magnetite and epidote rich bands |
| 372 | coarse grain granite, amphibolitic |

Province: Western
Locality: Machili
Borehole: GS 108

Site latitude: 16° 52' S
Site longitude: 25° 09' E
Site elevation: 1095 ± 5 m
Completed by: November 14, 1968
Surveyed on: August 18, 1971
Dip angle: 90°

Depth range: 164-302 m
N: 13
Conductivity 3.00 ± 0.08
Gradient: 22.3 ± 3.5
Heat flow 67 ± 11

| depth (m) | T (°C) |
|---|---|
| 19.3 | 24.48 |
| 29.4 | 24.62 |
| 39.6 | 25.02 |
| 49.8 | 25.40 |
| 59.9 | 25.82 |
| 70.2 | 26.24 |
| 80.4 | 26.77 |
| 90.7 | 27.92 |
| 101.1 | 28.35 |
| 111.6 | 28.56 |
| 122.1 | 28.96 |
| 132.6 | 29.33 |
| 143.4 | 29.72 |
| 154.1 | 30.16 |
| 164.8 | 30.45 |
| 175.5 | 30.70 |
| 186.3 | 30.99 |
| 197.0 | 31.24 |
| 207.6 | 31.55 |
| 217.9 | 31.76 |
| 228.2 | 31.99 |
| 238.8 | 32.24 |
| 249.0 | 32.47 |
| 259.5 | 32.71 |

| depth (m) | k (W/mK) |
|---|---|
| 61 | 3.08 |
| 70 | 2.94 |
| 85 | 3.82 |
| 95 | 3.07 |
| 110 | 2.96 |
| 122 | 3.15 |
| 137 | 3.00 |
| 160 | 2.90 |
| 185 | 2.75 |
| 205 | 2.73 |
| 225 | 2.93 |
| 250 | 2.85 |
| 286 | 3.07 |
| (temperatures continued) | |
| 270.0 | 32.92 |
| 280.6 | 33.14 |
| 291.2 | 33.34 |
| 302.0 | 33.52 |

| to depth (m) | geology |
|---|---|
| 11 | unconsolidated Barotse sand |
| 65 | ferruginous sandstone |
| 87 | yellow sandstone |
| 98 | pink sandstone |
| 103 | red mudstone |
| 107 | pink sandstone |
| 110 | red mudstone |
| 150 | red sandstone |
| 159 | red mudstone |
| 304 | red sandstone |

## REFERENCES


Abramowitz, M. and Stegun, I. A., 1966. Handbook of Mathematical Functions with Formulas, Graphs, and Mathematical Tables. National Bureau of Standards Applied Mathematics Series - 55, Washington, 1046 pp.

Andrews, E. M., 1974. Gravity survey of Malawi: fieldwork and processing. Inst. Geol. Sciences. London Report 74/15.

Baker, B. N. and Wohlenberg, J., 1971. Structure and evolution of the Kenya rift valley. Nature, 229: 538-542.

Banks, R. J. and Ottey, P., 1974. Geomagnetic deep sounding in and around the Kenya rift valley. Geophys. J., 36: 321-335.

Beck, A. E., 1965. Techniques of measuring heat flow on land. In: W. H. K. Lee (Editor), Terrestrial Heat Flow, Geophysical Monograph Series No. 8. American Geophysical Union, Washington, pp. 24-57.

Beck, A. E. and Mustonen, E., 1972. Preliminary heat flow from Ghana. Nature Physical Science, 235: 172-174.

Beer, J. H. de, Gough, D. I. and van Zijl, J. S. V., 1975. An electrical conductivity anomaly and rifting in southern Africa. Nature, 255: 678-680.

Beers, Y., 1962. Introduction to the Theory of Error. Addison-Wesley, Reading, Mass.

Birch, F., 1950. Flow of heat in the Front Range, Colorado. Geol. Soc. Am. Bull., 61: 567-630.

_____. 1954. Heat from radioactivity. In: H. F. Faul (Editor), Nuclear Geology. John Wiley and Sons, New York, p. 148.

Birch, F., Roy, R. F. and Decker, E. R., 1968. Heat flow and thermal history in New England and New York. In: W. White and E-an Zen (Editors), Studies of Appalachian Geology: Northern and Maritime. Interscience, New York, pp. 437-451.

Blackwell, D. D., 1971. The thermal structure of the continental crust. In: J. G. Heacock (Editor), The Structure and Physical Properties of the Earth's Crust, Geophysical Monograph Series No. 14. American Geophysical Union, Washington, pp. 169-184.

Briden, J. C. and Gass, I. G., 1974. Plate movement and continental magmatism. Nature, 248: 650-653.

Bullard, E. C., 1939. Heat flow in South Africa. Proc. R. Soc. London, A, 173: 474-502.

Burke, K. and Wilson, J. T., 1972. Is the African plate stationary? Nature, 239: 387.

Cahen, L., 1970. Igneous activity and mineralization episodes in the evolution of the Kibaride and Katangide orogenic belts of Central Africa. In: African Magmatism and Tectonics. Oliver and Boyd, Edinburgh, 461 pp.

Cahen, L. and Snelling, N. J., 1966. The Geochronology of Equatorial Africa. North-Holland, Amsterdam, 195 pp.

Carslaw, H. S. and Jaeger, J. C., 1959. Conduction of Heat in Solids, 2nd edition. Oxford University Press, Oxford, 510 pp.

Carte, A. E., 1954. Heat flow in the Transvaal and Orange Free State. Proc. Phys. Soc. B, 67: 664-672.

Carte, A. E. and van Rooyen, A. I. M., 1971. Further measurements of heat flow in South Africa. J. Mine Ventilation Soc. South Africa, July: 94-98.

Chapman, D. S. and Pollack, H. N., 1974. Cold spot in West Africa: anchoring the African plate. Nature, 250: 477-478.

Chapman, D. S., Vise, J. and Pollack, H. N., 1975. Geothermal investigations in Zambia. J. Engin. Inst. Zambia, 19, 3: 33-37.

Clifford, T. N., 1967. The Damaran episode in the Upper Proterozic - Lower Paleozoic structural history of southern Africa. Spec. Pap. Geol. Soc. Amer., 92: 100 pp.

_____. 1968. Radiometric dating and the pre-Silurian geology of Africa. In: E. I. Hamilton and R. M. Farquhar (Editors), Radiometric Dating for Geologists, Interscience, London, pp. 299-416.

Decker, E. R. and Smithson, S. B., 1975. Heat flow and gravity interpretation across the Rio Grande rift in southern New Mexico and West Texas. J. Geophys. Res., 80: 2542-2552.

Degens, E. T., von Herzen, R. P. and Wong, H. K., 1971. Lake Tanganyika: water chemistry, sediments, geologic structure. Naturwissenschaften, 58: 229-240.

Degens, E. T., von Herzen, R. P., Wong, H. K., Deuser, W. G. and Jannasch, H. W., 1973. Lake Kivu: structure, chemistry and biology of an East African rift lake. Geol. Rundschau, 62: 245-277.

Dietz, R. S. and Holden, J. C., 1970. The breakup of Pangea. Scientific American, 223: 30-41.

Diment, W. H., Urban, T. C., Sass, J. H., Marshall, B. V., Munroe, R. J. and Lachenbruch, A. H., 1975. Temperatures and heat contents based on conductive transport of heat. In: D. E. White and D. L. Williams (Editors), Assessment of Geothermal Resources of the United States - 1975. Geological Survey Circular 726: 84-103.

Drysdall, A. R., Johnson, R. L., Moore, T. A. and Thieme, J. G., 1972. Outline of the geology of Zambia. Geologie en Mijnbouw, 51 (3): 265-276.

Evans, T. R. and Tammemagi, H. Y., 1974. Heat flow and heat production in northeast Africa. Earth Planet. Sci. Lett., 23: 349-356.

Fairhead, J. D. and Girdler, R. W., 1969. How far does the Rift System extend through Africa? Nature, 221: 1018-1020.

Fairhead, J. D. and Girdler, R. W., 1971. The seismicity of Africa. Geophys. J., 24: 271-301.

Florensov, N. A., 1969. Rifts of the Baikal mountain region. Tectonophysics, 8: 443-456.

Garrard, P., 1968. The geology of the Chainama Hills area: explanation of degree sheet 1528, NW quarter. Rep. Geol. Surv. Zambia, 24: 80 pp.

Girdler, R. W., 1970. A review of Red Sea heat flow. Phil. Trans. R. Soc. Lond. A, 267: 191-203.

_____. 1975. The great negative Bouguer gravity anomaly over Africa. Trans. Amer. Geophys. Union, 56: 516-519.

Gough, D. I., 1963. Heat flow in the southern Karroo. Proc. R. Soc. London. A, 272: 207-230.

Gumper, F. and Pomeroy, P. W., 1970. Seismic wave velocities and earth structure on the African continent. Bull. Seismol. Soc. Am., 60: 651-668.

Haenel, R., 1970. Interpretation of the terrestrial heat flow in the Rhinegraben. In: J. H. Illies and St. Mueller (Editors), Graben Problems. International Upper Mantle Project, Scientific Report No. 27, pp. 116-120.

Heezen, B. C., 1969. The world rift system: an introduction to the symposium. Tectonophysics, 8: 269-279.

Heier, K. S. and Rogers, J. W., 1963. Radiometric determination of thorium, uranium and potassium in basalts. Geochim. Cosmochim. Acta, 27: 137-154.

Illies, J. H., 1972. The Rhinegraben rift system - plate tectonics and transform faulting. Geophys. Surveys, 1: 27-60.

Jaeger, J. C., 1970. Heat flow and radioactivity in Australia. Earth Planet. Sci. Lett., 8: 285-292.

Jaeger, J. C. and Beck, A., 1955. The calculation of heat flow through disks and its application to conductivity measurements. Br. J. Appl. Phys., 6: 15-16.

Jessop, A. M., 1968. Three measurements of heat flow in eastern Canada. Can. J. Earth. Sci. 5: 61-68.

Jessop, A. M., Sclater, J. G. and Hobart, M. A., 1975. World heat flow data collection. Geothermal Series, Earth Physics Branch, Ottawa, in preparation.

Kennedy, W. Q., 1965. The influence of basement structure on the evolution of the coastal (Mesozoic and Tertiary) basins of Africa. In: Salt Basins around Africa. London, Institute of Petroleum. 7-16.

Khan, M. A. and Mansfield, J., 1971. Gravity measurements in the Gregory rift. Nature Physical Science, 229: 72-75.

Lachenbruch, A. H. and Brewer, M. C., 1959. Dissipation of the temperature effect in drilling a well in Arctic Alaska. U. S. Geol. Surv. Bull., 1083-C:73-109.

Lee-Potter, J. B., 1961. Roan Muliashi Basin - Baluba. In: F. Mendelsohn (Editor), The Geology of the Northern Rhodesian Copperbelt. Macdonald, London, pp. 343-350.

Lubimova, E. A., 1969. Heat flow patterns in Baikal and other rift zones. Tectonophysics, 8: 457-467.

Maasha, N. and Molnar, P., 1972. Earthquake fault parameters and tectonics in Africa. J. Geophys. Res., 77: 5731-5743.

Mendelsohn, F. (Editor), 1961. The Geology of the Northern Rhodesian Copperbelt. Macdonald, London, 523 pp.

Money, N. J., 1972. An outline of the geology of western Zambia. Rec. Geol. Surv. Zambia, 12: 103-123.

Morgan, P., 1973. Terrestrial heat flow studies in Cyprus and Kenya. Ph.D. Thesis, University of London, 346 pp.

Morgan, P., Williamson, K. H., Evans, T. R. and Wheildon, J., 1973. Preliminary heat flow studies in and around the Kenya rift. Abstracts of the first meeting of the European Geophysical Society, Zurich: 71.

Piper, J. D. A. and Richardson, A., 1972. The paleomagnetism of the Gulf of Guinea volcanic province, West Africa. Geophys. J. 29: 147-151.

Pollack, H. N. and Chapman, D. S., 1974. To what extent does the lithosphere mask lateral variations of temperature in the asthenosphere? Trans. Amer. Geophys. Union, 55: 1193.

Polyak, B. G. and Smirnov, Ya. B., 1968. Relationship between terrestrial heat flow and the tectonics of continents. Geotectonics, 4: 205-213.

Rao, R. U. M. and Jessop, A. M., 1975. A comparison of the thermal character of shields. Can. J. Earth Sci., 12: 347-360.

Ratcliffe, E. H., 1959. Thermal conductivities of fused and crystalline quartz. Brit. J. Appl. Phys., 10: 22-25.

Reeves, C. V. and Hutchins, D. G., 1975. Crustal structures in central southern Africa. Nature, 254: 408-410.

Reiter, M., Edwards, C. L., Hartman, H. and Weidman, C., 1975. Terrestrial heat flow along the Rio Grande rift, New Mexico and southern Colorado. Geol. Soc. Amer. Bull., 86: 811-818.

Roy, R. F., Decker, E. R., Blackwell, D. D. and Birch, F., 1968 a. Heat flow in the United States. J. Geophys. Res., 73: 5207-5221.

Roy, R. F., Blackwell, D. D. and Birch, F., 1968 b. Heat generation of plutonic rocks and continental heat flow provinces. Earth Planet. Sci. Lett., 5: 1-12.

Roy, R. F., Blackwell, D. D. and Decker, E. R., 1972. Continental heat flow. In: E. C. Robertson (Editor), The Nature of the Solid Earth. McGraw Hill, pp. 506-543.

Sass, J. H., Lachenbruch, A. H., Munroe, R. J., Greene, G. W. and Moses, T. H. Jr., 1971. Heat flow in the Western United States. J. Geophys. Res., 76: 6376-6413.

Sass, J. H. and Behrendt, J. C. Geothermal data from the Liberian Precambrian shield (in preparation).

Scholz, C. H., 1975. Evidence for incipient rifting in southern Africa. Trans. Amer. Geophys. Union., 56: 450 (abstract).

Scholz, C. H., Koczynski, T. A. and Hutchins, D. G., 1976. Evidence for incipient rifting in southern Africa. Geophys. J., (in press).

Shaw, D. M., 1967. U, Th, and K in the Canadian Precambrian shield and possible mantle compositions. Geochim. Cosmochim. Acta, 31: 1111.

Sletene, R. L., Wilcox, L. E., Blouse, R. S. and Sanders, J. R., 1973. Bouguer gravity anomaly map of Africa. Tech. Paper 73-3, U. S. Defense Mapping Agency.

Smith, A. G., 1963. The geology of the country around Mazabuka and Kafue: explanation of degree sheets 1527, SE quarter, and 1528, SW quarter. Rep. Geol. Surv. N. Rhodesia, 2: 32 pp.

Snelling, N. J., Hamilton, E. I., Drysdall, A. R. and Stillman, C. J., 1964. A review of age determinations from Northern Rhodesia. Econ. Geol., 59: 961-981.

Snelling, N. J., Johnson, R. L. and Drysdall, A. R., 1972. The geochronology of Zambia. Rec. Geol. Surv. Zambia, 12: 19-30.

Smithson, S. B. and Decker, E. R., 1974. A continental crustal model and its geothermal implications. Earth Planet. Sci. Lett., 22: 215-225.

Sowerbuts, W. T. C., 1969. Crustal structure of the East African plateau and rift valleys from gravity measurements. Nature, 223: 143-146.

Stillman, C. J., 1965. The geology of the Musofu river and Mkushi areas: explanation of degree sheet 1329, part of NW quarter and SW quarter. Rep. Geol. Surv. Zambia, 12: 52 pp.

Swanberg, C. A., Chessman, M. D., Simmons, G., Smithson, S. B., Gronlie, G. and Heier, K. S., 1974. Heat flow-heat generation studies in Norway. Tectonophysics, 23: 31-48.

Swardt, A. M. J. de and Drysdall, A. R., 1964. Precambrian geology and structure in central Northern Rhodesia. Geol. Surv. Northern Rhodesia Mem., 2: 82 pp.

Swardt, A. M. J. de. and Simpson, J. G., 1972. A structural interpretation for part of Zambia. Rec. Geol. Surv. Zambia, 12: 31-35.

Von Herzen, R. P. and Vacquier, V., 1967. Terrestrial heat flow in Lake Malawi, Africa. J. Geophys. Res., 72: 4221-4226.

Wohlenberg, J., 1975. Geophysikalische Aspekte der Ostafrikanischen Grabenzonen. Geologisches Jahrbuch E., 4: 82 pp.